Classification of the emerging freeform three-dimensional printing techniques

Arthur Colly, Christophe Marquette, Jean-Marc Frances, Edwin-Joffrey Courtial

Classification of the emerging Freeform 3D printing techniques

Arthur COLLY[1-2] (ID : 0000-0001-9820-5845), Christophe MARQUETTE[1] (ID : 0000-0003-3019-0696), Jean-Marc FRANCES[2] (ID : 0000-0002-3734-4793), Edwin-Joffrey COURTIAL[1]* (ID : 0000-0002-1406-5871)

1. 3d.FAB, Univ Lyon, CNRS, UCBL, ICBMS, UMR5246, ICBMS, 69622 Villeurbanne, France.
2. Elkem Silicones, 55 Av. des Frères Perret, 69192, Saint-Fons Cedex, France

**Corresponding author at:* 3d.FAB, Univ Lyon, Université Lyon1, CNRS, INSA, CPE-Lyon, ICBMS, UMR 5246, 43, Bd du 11 novembre 1918, 69622 Villeurbanne cedex, France
E-mail address: edwin.courtial@univ-lyon1.fr

Abstract

Freeform 3D printing technique is a promising additive manufacturing field, enabling researchers to produce complex shapes with advanced materials. Mainly used for soft material deposition within a support matrix, these techniques were able to overcome issues encountered in classical additive manufacturing processes, mainly related to lack of self-supporting properties. Numerous Freeform 3D printing works were performed since its initial proposition, associated to an equal number of process names and acronyms, leading the scientific community to declension or misuse of definitions or terms. To overcome this lack of standardization, the present review gathers the existing Freeform 3D printing techniques to define six clear classes, also including the processes that were not explicitly termed in their original reports. This review provides also a brief overview of application domains where Freeform 3D printing appears as an important asset to go further in the manufacturing of soft matter.

Graphical abstract

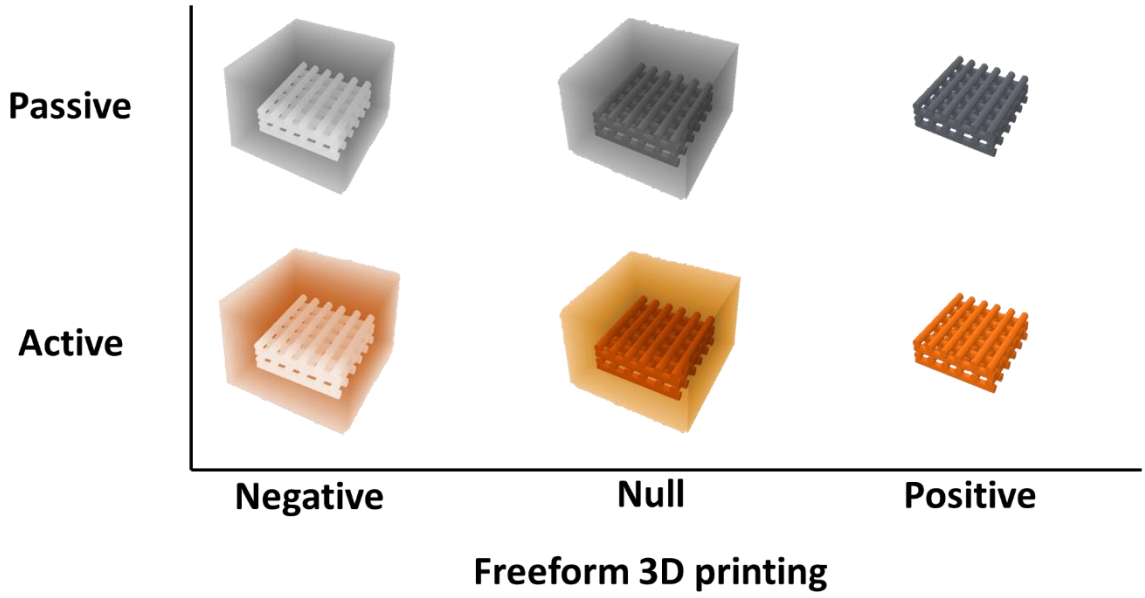

Keywords

Freeform 3D printing, classification, support matrix, Soft matter, Additive manufacturing

Declarations

Funding

This study was conducted within the IMC project co-funded by Elkem Silicones and the French Ministry of National Education and Technological Research (Grant Number 2019/1950).

Conflicts of interest/Competing interests

All other authors declare that they have no competing interests.

Availability of data and material

Not applicable

Code availability

Not applicable

Abbreviations

3D printing: Three-dimensional printing
4D printing: Four-dimensional printing
AAFB: Aspiration-Assisted Freeform Bioprinting
ABS: Acrylonitrile Butadiene Styrene
Ad-HA: Adamantane modified hyaluronic acid
AAM: Acrylamide
BATE: Bioprinting-Assisted Tissue Emergence
CD-HA: β-cyclodextrin modified hyaluronic acid
CLASS: Constructs Laid in Agarose Slurry Suspension
CMT: Critical micelle temperature
COBICS: Ceramic Omnidirectional Bioprinting In Cell-Suspensions
DF3DP: Direct Freeform 3D Printing Process
DIW: Direct Ink Writing
EDIW: Embedded Direct Ink Writing
EDTA: Ethylenediaminetetraacetic acid
EIW: Embedded Ink Writing
Emb3D: Embedded 3D Printing
F127: Pluronic® F-127
FPP: Freeform Polymer Precipitation
FRE: Freeform Reversible Embedding
FREAL: Freeform Reconfigurable Embedded All-Liquid
FRESH: Freeform Reversible Embedding of Suspended Hydrogels
GelMA: Gelatin methacrylate
GHost writing: Guest-Host writing
HA: Hyaluronic acid
HA-BP: Bisphosphonate functionalized hyaluronic acid
HIPS: High impact polystyrene
IBPC: In-Bath Print and Cure
LDM: Liquid Deposition Modeling
LLS: Liquid-Like-Solid
MITCH: Mixing-Induced Two-Composite Hydrogels
NaCl: Sodium chloride
NIPAM: Poly-N-isopropylacrylamide
Nor-HA: Norbornene-modified hyaluronic acid
O_2: Dioxygen
ODP: Omnidirectional Printing
PAA: poly(acrylic acid)
PCL: Polycaprolactone

PDMS: Polydimethylsiloxane

PEG: Poly(ethylene glycol)

PEGDA: Poly(ethylene glycol) diacrylate

PEO: Poly(ethylene oxide)

PIV: Particle Image Velocimetry

PLA: Polylactic acid

PPO: Poly(propylene oxide)

PTFE: Poly(tetrafluoro ethylene)

PTG: Printing-Then-Gelation

PVA: Poly(vinyl alcohol)

PVB: Poly(vinyl butyral)

RLP: Rapid Liquid Printing

SCC: Sub Surface Catalyzation

SEBS: Polystyrene-block ethylene/butylene-block-polystyrene

SEP: Polystyrene-block ethylene/propylene

SLA: Stereolithography

SLAM: Suspended Layer Additive Manufacturing

SMAP: Solid Matrix-Assisted 3D Printing

SWIFT: Sacrificial Writing Into Functional Tissue

TMF: Triggered Micropore-Forming

1. Introduction

Additive manufacturing or 3D printing enables the design and fabrication of complex objects which were hardly feasible using classical molding approaches. Since its initial development in the 1980's [1], several techniques were implemented or invented that handle a large variety of raw materials. In the particular case of liquid raw materials (resins, thermosetting polymers, silicones, bioinks, etc.), the developed additive technologies were either based on Stereolithography or Direct Ink Writing (DIW) (sometimes called Liquid Deposition Modelling (LDM), cold extrusion or microextrusion) [2–5]. However, in most cases, the rheological and mechanical properties of the liquid raw material are incompatible with the DIW process since the material itself, once deposited, is unable to withstand its own weight [6–8].

Rapid solidification of the material, typically through photo-polymerization, thermal, ionic or chemical crosslinking [9], can be a solution for these raw materials. However, this remains partially unsatisfying for many materials or applications incompatible with photochemistry or metal ions (implantable material, unmodified biopolymers, bioprinting, etc.) [7,9]. Moreover, with their low elastic modulus (typically under 100 kPa) these raw materials undergo deformation under small perturbations induced by the printing process, leading to recurrent fidelity loss [6,10].

One of the most promising technique to overcome this challenge is the Freeform 3D printing [2,10–12], defined as a variant of the DIW [13], where liquid raw materials (generally termed "ink") are directly deposited within a temporary or permanent second material. This second material (generally termed "support matrix" or "bath") provides a supporting environment which prevents gravitational collapse and then enables Freeform, but also, in the best conditions, optimizes surface tension to ensure high print fidelity. The liquid raw materials should minimally diffuse within the second material to keep this high print fidelity during and after Freeform 3D printing [14]. Since its first mention in literature in 2011 [13], Freeform 3D printing has been widely studied and incremented with more than twenty different types of support matrices [2]. The numerous studies performed consolidated a strong understanding of the rheological phenomena and of the occurring instabilities in place [2,10] but also of the potential applications [15,16].

Nevertheless, as highlighted by Shiwarski [16], even if the knowledge and information are here, the Freeform 3D printing remains a young growing field of research where "there is a lack of standardization in the 3D bioprinting field". In the 3D printing field, taxonomy is barely organized and a clear categorization is required. Numerous terms are for example used to describe Freeform 3D printing techniques, and the lack of classification leads the scientific community to declension or misuse of definitions or terms. An early stages classification effort was proposed by Compaan [17] where the "printing-then-gelation" (PTG) concept was used to cover only the two main Freeform techniques, i.e. FRESH (Freeform Reversible Embedding of Suspended Hydrogels) [16,18] and writing in granular medium [12]. In a more generic approach, *Chen et al.* [2] termed the technique "Freeform 3D printing", where the material (ink) is deposited within a support (matrix). This term, simple and generic, have been already adopted by the community (Freeform Reversible Embedding [11], Freeform Polymer Precipitation [19], Direct Freeform 3D Printing Process [20], 3D Freeform printing of silk fibroin, etc. [21]). Unfortunately, this term also appears in other 3D printing fields not using liquid raw material deposition, i.e. electron beam based Freeform 3D printing of titanium alloy or Freeform fabrication of thermoplastics by cleverly using a 6-axis bed plate, bringing more degrees of freedom of the construct [22,23].

This lack of specificity often leads to some misconceptions and Chen *et al.* [2] attempt a more precise classification of the main Freeform 3D printing processes in three categories: positive; negative and functional. Segregation being performed according to which material (ink or matrix) composed the final product. When the final product is the ink material the classification is "positive", when the final product is the matrix the classification is "negative" and when then final product is a consequence of a reaction between ink and matrix, the classification is "functional". However, recent works in the field were found to be impossible to be described clearly and fully by the existing classification and the aim of the present review is to propose a refined, comprehensive and more detailed classification, enabling the scientific community to clarify the position of past and future Freeform 3D printing techniques.

2. Classification of Freeform 3D printing techniques

Figure 1 reviews and classifies exhaustively the existing Freeform 3D printing techniques. Since its initial development, Freeform 3D printing expanded in various fields, from silicones to biomaterials, from inactive 3D shapes to living tissues bioprinted [16]. The printing processes were mostly extrusion-based processes but other additive manufacturing methods were also studied such as inkjet [24,25] or pick and place (aspiration-assisted) [26]. In this review, the Freeform 3D printing techniques are classified into a 2-entries matrix of 6 categories: entry #1: negative, null, and positive Freeform 3D printing; entry #2: passive and active Freeform 3D printing. "Negative" Freeform 3D printing defines techniques where the final product is the matrix and the sacrificial ink is removed, "null" where both matrix and ink are kept and "positive" where the final product is the ink and the sacrificial matrix is removed. In addition, "passive" sub-category defines where ink and matrix do not chemically interact and "active" sub-category defines techniques where ink and matrix affect each other.

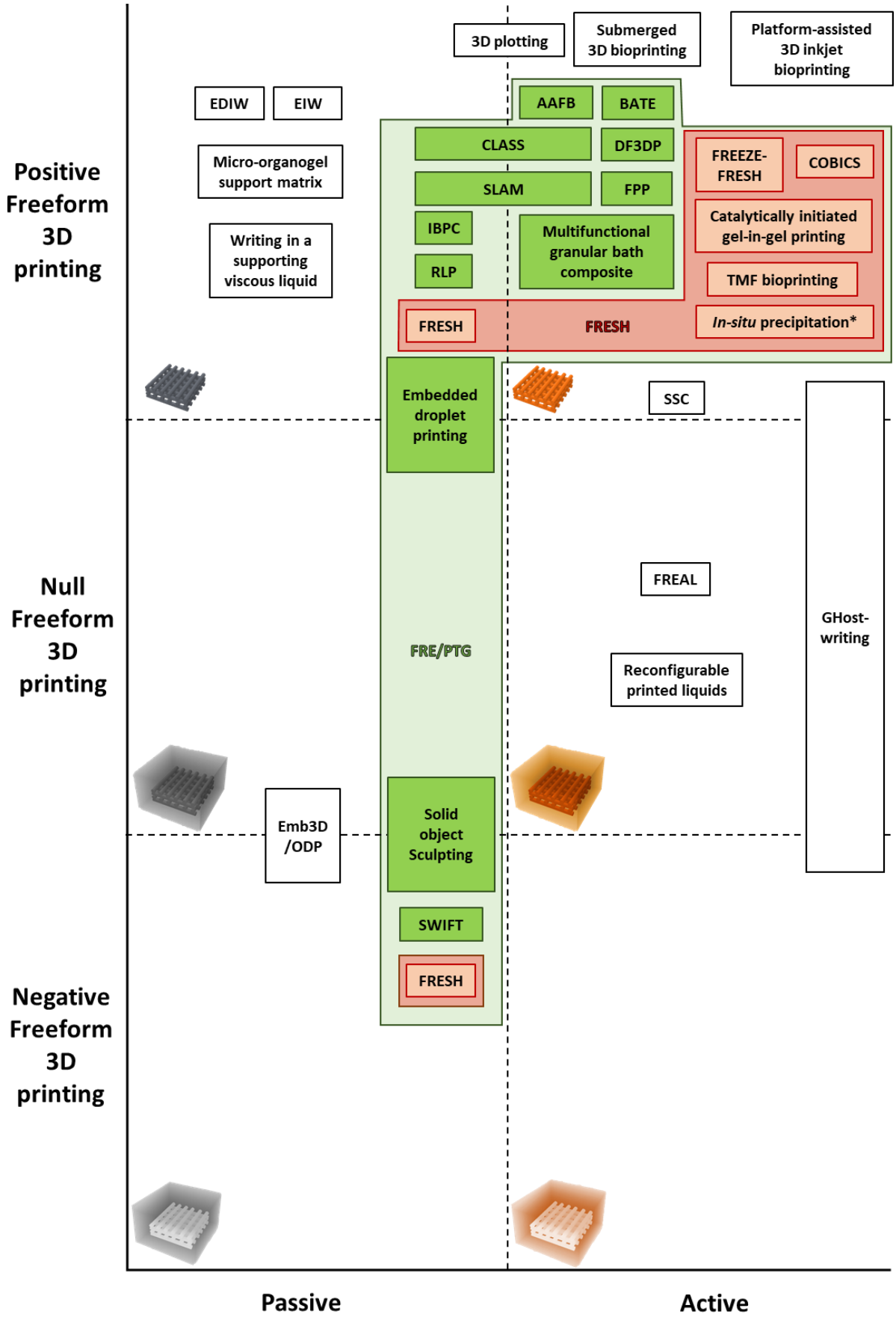
Positive Freeform 3D printing
Null Freeform 3D printing
Negative Freeform 3D printing
Passive
Active
3D plotting
Submerged 3D bioprinting
Platform-assisted 3D inkjet bioprinting
EDIW
EIW
Micro-organogel support matrix
Writing in a supporting viscous liquid
AAFB
BATE
CLASS
DF3DP
SLAM
FPP
IBPC
RLP
Multifunctional granular bath composite
FRESH
FRESH
FREEZE-FRESH
COBICS
Catalytically initiated gel-in-gel printing
TMF bioprinting
In-situ precipitation*
Embedded droplet printing
SSC
FREAL
GHost-writing
FRE/PTG
Reconfigurable printed liquids
Emb3D /ODP
Solid object Sculpting
SWIFT
FRESH

62

Figure 1. Classification map of existing Freeform 3D printing techniques. Distinction between the different categories from negative, null to positive on the vertical axis (Entry #1). Distinction between the two sub-categories from passive to active on the horizontal axis (entry #2) with the corresponding schemes. Each techniques are displayed and gathered within their respective families represented by the colored boxes. The green box gathers the techniques belonging to the FRE/PTG (Freeform Reversible Embedding/Printing Then Gelation) class and the red box, the techniques belonging to the FRESH (Freeform Reversible Embedding of Suspended Hydrogels) technique where FRE/PTG encompasses the FRESH technique. For a better visibility the in-situ precipitation coupled FRESH 3D printing technique was shortened and marked with an asterisk.

3. Negative Freeform 3D printing

In the negative Freeform 3D printing [2] (**Figure 1**), the matrix is the final product and is generally permanently solidified. The ink, often referred as sacrificial or fugitive, is extruded within the matrix with high spatial control allowing unprecedented complex shape formation. Removal of the ink is performed by temperature change [13,27], dissolution in a static fluid or gas flow [28–30], yielding constructs characterized by the presence of controlled cavities (**Figure 2A**). In the case of passive negative Freeform 3D printing (ink and matrix do not impact chemically), smooth and detailed cavities can be manufactured by extruding non-miscible materials [13,27]. On the contrary, in active negative Freeform 3D printing (ink and matrix impact chemically each other), an interphase is created between the ink and the matrix stabilizing the construct but need to be removed with more extended washings [30,31]. The matrix is usually designed to have a yield stress behavior. At rest, under no applied shear stress, the matrix exhibits a solid behavior while upon shearing during 3D printing, the matrix starts to flow, enabling the motion of the printing tip. Rheological properties of this material are then conditioning the negative Freeform 3D printing performances. An optimum have to be found to achieve suspending [10], tip displacement, self-healing to avoid crevasse generation affecting the printing fidelity [12,32] and other instabilities around moving tip and filament, well defined in other reports [2,33,34].

Several studies used such yield stress matrices for negative Freeform 3D printing and will be developed in the next sections. The classification will present separately passive negative Freeform 3D printing and active negative Freeform 3D printing.

3.1. Passive negative Freeform 3D printing

3.1.1. Emb3D/ODP: Embedded 3D printing/ Omnidirectional printing

Omnidirectional printing (ODP) was first proposed by Wu *et al.* [13] for developing biomimetic microvascular constructs (**Figure 2B**). Passive negative Freeform 3D printing was here performed within a diacrylate-modified form of Pluronic® F-127 (F127), enabling its subsequent photopolymerization. Interestingly, unmodified F127 was also used as a sacrificial ink and removed by lowering the temperature.

In the Wu *et al*. experiments, the yield stress properties of the synthesized diacrylate-modified F127 hydrogel were maladapted and crevasses were generated during the tip displacement. To overcome this issue, a fluid layer of diacrylate-modified F127 was used to overlie the suspending material and fill in real time the forming crevasses.

This technique was further upgraded and transposed to silicone matrices for creating autonomous moving soft robots. The soft autonomous robots' movements were triggered by propellant combustion controlled by microfluidic logic [27].

3.1.2. FRE/PTG: Freeform Reversible Embedding/Printing-Then-Gelation

Compaan *et al.* [35] developed an innovative composite matrix composed of packed microgels of gellan or gelatin within a continuous gelatin solution. The matrix is crosslinked by the use of transglutaminase that form isopeptide bonds between two protein molecules found in gelatin [36]. Varying the nature of the microgel as well as its volume fraction enabled the authors to tune both mechanical and biological properties of the final composite

construct. The composite matrix was shown to support cell culture and tissue development. A demonstration of the capability of the technique to produce interconnected perfusion channels was performed using alginate as fugitive ink, subsequently removed by solubilisation in water, PBS or sodium citrate solution (**Figure 2C**). Similarly, Mooley *et al.* proposed a matrix composed of cell-laden gelatin methacrylate (GelMA) microgel within a 1 wt% GelMA solution, enabling its subsequent photopolymerization [37]. In an *in-vitro* disease and tumor modeling application, authors created a tumor microenvironment by printing tumor cell aggregates and fugitive F127 ink to generate endothelialized channels. The growth and invasive potential of the tumor models towards the vasculature as a function of spatial location were monitored providing the understanding of disease and drug development.

3.1.3. SWIFT: Sacrificial Writing Into Functional Tissue

An interesting application of passive negative Freeform 3D printing in the field of tissue engineering was developed based on a matrix composed of 212 µm diameter cell spheroids derived from patient [38]. The sacrificial ink was here composed of gelatin, removed to form interconnected perfusion channels through heating at 37°C (**Figure 2D**). The obtained living system was shown to enable long-term tissue maturation (8 days) and to exhibit native tissue functionalities. As proofs of concept, perfused vascular constructs and contractile cardiac tissues were demonstrated. This technique using a granular, microparticle suspension matrix, is considered in this review as a sub category of the FRE-PTG technique (paragraph 5.1.1).

3.1.4. Other passive negative Freeform 3D printing systems

Another technique was built using passive negative Freeform 3D printing but is not explicitly named. Shin and Hyun [28] reported a novel green matrix based on cellulose nanofiber derived from wood for two-dimensional microfluidic systems (**Figure 2E**). They developed the unique concept of fabricating thin deformable film useful to prepare paper-like microfluidic systems by drying the matrix after Freeform patterning. The fugitive ink was here a nonpolar material composed of petroleum gelly and paraffin, eliminated under air pressure and n-hexane washing.

Since the approach was targeting microfluidic applications, the authors smartly developed a method to waterproof the opened channels through a coating with silicone elastomer to prevent fluid diffusion in the soft film when perfused. The paper-like microfluidic device that was used as pH and metal sensor detection, can be stackable and interconnectable with other microfluidic sheets.

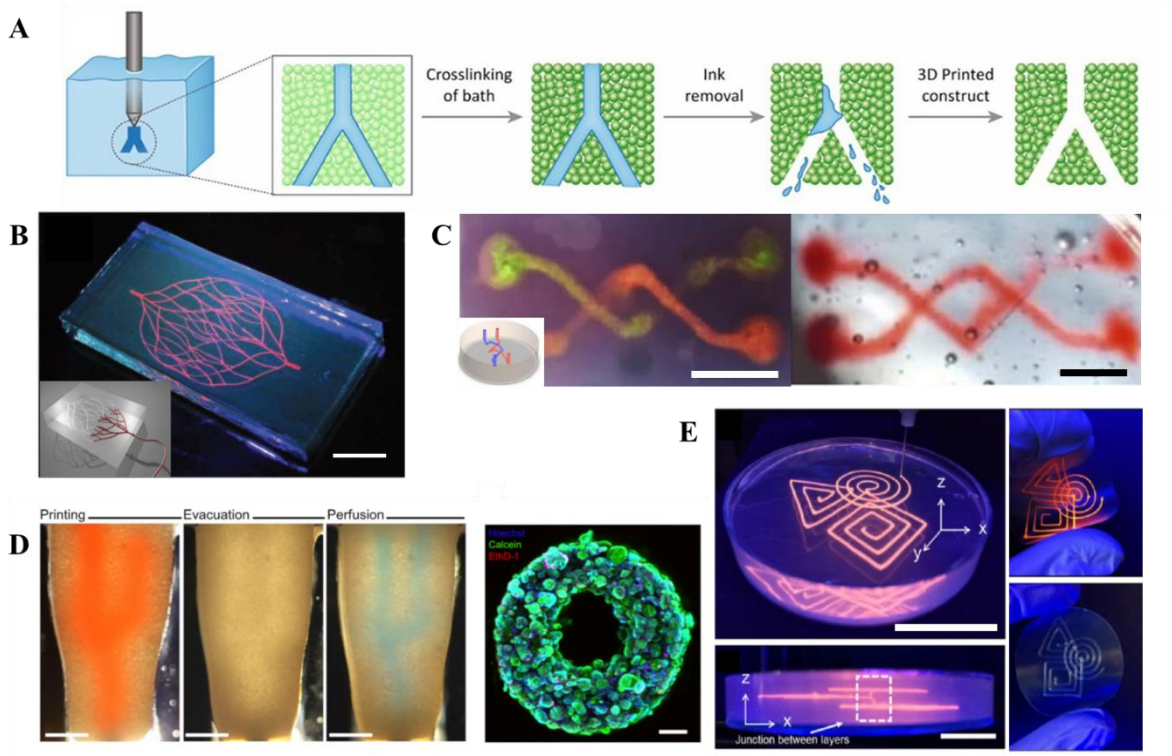

Figure 2. Overview of the structures obtained using passive negative Freeform 3D printing. (A) Principle of channel, cavities formation where the fugitive ink is extruded within the matrix and then removed after matrix solidification. Adapted with permission from *[39]*. Copyright 2020, ELSEVIER. (B) 3D microvascular network composed of F127 fugitive ink (dyed in red) within a F127-DA crosslinked matrix. Scale bar 10 mm. Adapted with permission from *[13]*. Copyright 2011, WILEY-VCH. (C) 3D Twisted channels of fugitive alginate ink printed within gelatin-gellan (left) and gelatin-gelatin (right) composite matrix. Scale bars 5 mm. Adapted with permission from *[35]*. Copyright 2020, ACS. (D) Passive negative Freeform 3D printing of fugitive gelatin ink and perfusion within cardiac spheroid matrix. Right: Viability staining of the cardiac spheroids after 24h of perfusion (cross section). Scale bars 2 mm (left images) and 0.5 mm (right). Adapted with permission from *[38]*. Copyright 2019, AAAS. (E) Fabrication of a microfluidic system in a cellulose nanofiber matrix. Scale bars 0.5 mm. Adapted with permission from *[28]*. Copyright 2017, ACS.

3.2. Active negative Freeform 3D printing

3.2.1. FRESH: Freeform Reversible Embedding Of Suspended Hydrogels

FRESH, mostly used in positive Freeform 3D printing (paragraph 5.1.4) was modified for the fabrication of perfusable networks through negative Freeform 3D printing [29]. The matrix is composed of jammed gelatin microparticles in suspension and the sacrificial ink composed of xanthan gum removed by rinsing with water. Here, the matrix solidification was obtained simply by lowering the temperature below 25°C, without the need of covalent crosslinking. At the interface of the calcium-loaded gelatin matrix and the xanthan gum, a thin layer of calcium-xanthan gum was created [40], stable enough during the photocrosslinking of the matrix. Thin 0.6 mm diameter vessels were obtained. The authors showed that the obtained resolution was directly related to the gelatin

particles diameter (**Figure 3A**). Interestingly, the authors also demonstrated the use of jammed alginate microparticles as suspending matrix, solidified through calcium ions chelation.

3.2.2. GHost writing: Guest-host writing

The GHost writing (condensation of Guest-Host writing) technique was proposed by Highley *et al.* [41] and is based on an original chemical design named guest-host interactions. In this approach, a self-healing matrix is produced through the rapid, non-covalent and reversible supramolecular assembly of macromolecular chains, mainly composed of modified hyaluronic acid (adamantane or cyclodextrin). The weak bonds between adamantane and cyclodextrin can be disturbed by shear, allowing these materials to be used as Freeform 3D printing matrices (**Figure 3B**). In the frame of active negative Freeform 3D printing, a photocurable matrix was synthesized through the addition of norbornene moieties to the hyaluronic chains, enabling the photocrosslinking of the matrix after Freeform 3D printing. The ink used was also composed of adamantane or cyclodextrin hyaluronic acid, enabling the reversible interaction with the matrix. This interaction was the basis of the active property of the GHost technique since at the interface between ink and matrix, a thin layer of common composition was created, stable enough during the photocrosslinking of the matrix.
In a tissue engineering application of GHost writing, authors used hyaluronic acid further modified with adhesive peptides in order to promote cell adhesion and generate endothelialized microchannels [31] (**Figure 3C**). A continuous flux of growth factors diffusing into the hydrogel matrix was shown to promote angiogenesis, closely mimicking the vascularization of native tissues.

3.2.3. Other active negative Freeform 3D printing techniques

Xanthan-gum, an abundant and cost-effective natural polymer, was proposed for active negative Freeform 3D printing [30]. A photocurable methacrylate-functionalized xanthan gum was synthesized and used in conjunction with a sacrificial alginate ink removed using an EDTA solution (calcium sequestration). At the interface of the calcium loaded xanthan gum matrix and the alginate ink, a thin layer of calcium-alginate was created, stable enough during the photocrosslinking of the matrix. When cells were included inside the xanthan matrix, the active negative Freeform 3D printing led to perfused cellularized constructs with high cell viability and proliferation during 7 days (**Figure 3D**).

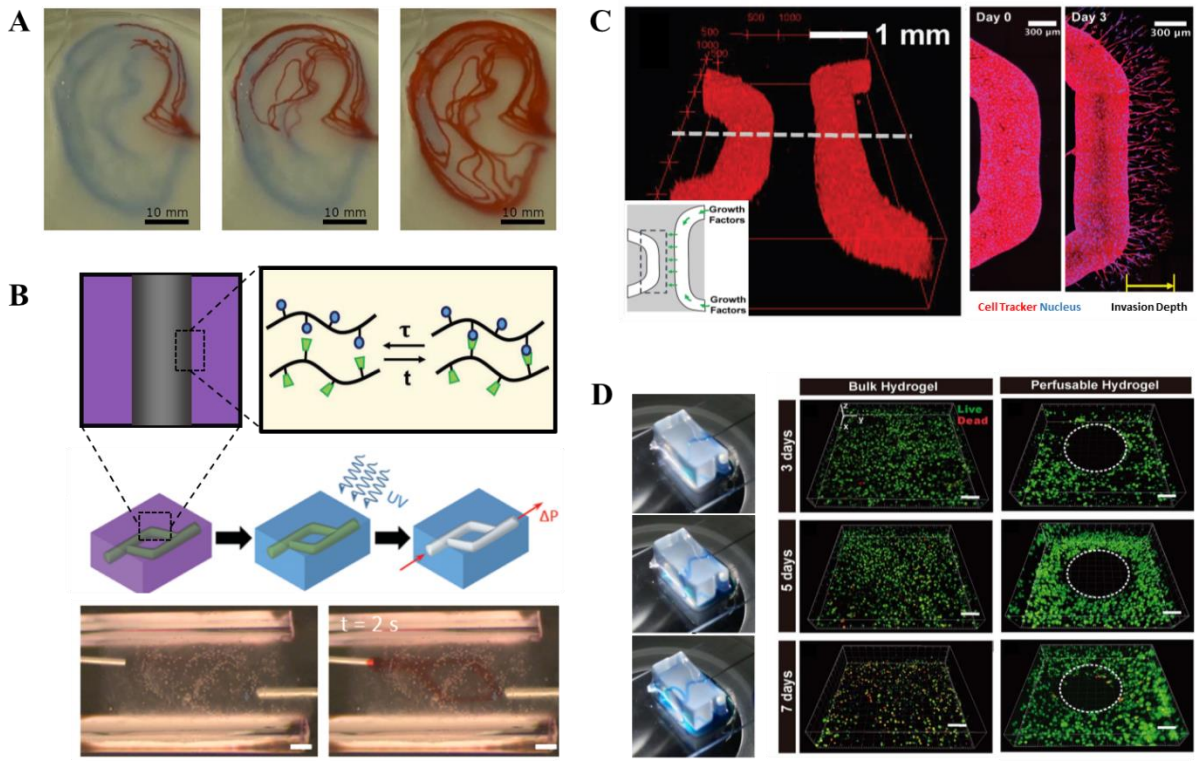

Figure 3. Overview of the printed structures using active negative Freeform 3D printing. (A) Perfusion, at different time interval, of an earlobe-shaped channels network within a gelatin microparticle matrix using fugitive xanthan gum. Scale bars 10 mm. Adapted with permission from *[29]*. Copyright 2018, MDPI. (B) Scheme of the supramolecular assembly of functionalized hyaluronic acid (adamantane or cyclodextrin) fugitive ink and photocurable matrix. Principle of channel formation by active negative Freefrorm 3D printing within guest-host hyaluronic-based matrix. Channel perfusion visualization at t=0 s and t=2 s. Scale bars 500 µm. Adapted with permission from *[41]*. Copyright 2015, WILEY-VCH. (C) Perfused microchannel for endothelialization under growth factor diffusion through the functionalized hyaluronic acid cell-degradable matrix. Progressive capillary invasion within the degradable matrix. Scale bars (left) 300 µm. Adapted with permission from *[31]*. Copyright 2018, WILEY-VCH. (D) Proof of perfusion of xanthan gum matrix and cross sections of encapsulated cells under perfusion for tissue maturation after 7 days. Alginate solution is used as sacrificial ink. Scale bars 500 µm (left) and 100 µm (right). Adapted with permission from *[30]*. Copyright 2020, IOP.

4. Null Freeform 3D printing

In null Freeform 3D printing, the final product is composed of both the extruded ink and the matrix, creating a multimaterial. The matrix is then generally permanently solidified, while the ink is either simply encapsulated within the matrix or also solidified. The non-permeability [33,42] and interfacial tension [43,44] of the ink/matrix system participate in the stability of the final multimaterial construct. Thus the ink remains embedded in the matrix but solidifying the matrix enhances the stability of the multimaterial enabling its handling under mechanical load [14,42,45]. This category has been explored in some studies for applications in the field of conductive composites or sensors [14,42], microchannels [44,46] and organ models for surgical training [47].

4.1. Passive null Freeform 3D printing

4.1.1. Embedded droplet printing

In this peculiar technique, no filament nor solid object is extruded. The system exploits the unwanted Rayleigh-Plateau instability encountered during Freeform printing [10]. This instability appears when the printed material and the supporting gel are immiscible. The developed interfacial tension creates then a destabilizing force that is in balance with the stabilizing force and the yield stress behavior of the gel. If the interfacial forces overcome the gel static yield stress, the printed material breaks into droplets. Yu and coworkers [43] used this instability to Freeform gallium-indium alloy droplets within a Carbopol® support matrix (**Figure 4A**). Intrinsically, metal has high surface tension, leading easily to droplet formation which size was shown to be controlled by the metal extrusion rate. On the contrary, droplet spacing was demonstrated to be related mainly to the Carbopol® rheological properties. Nelson and coworkers [45] published using the same principle, while naming this technique "embedded droplet printing", and deepened the understanding of the physicochemical mechanisms of droplet formation. Operating conditions were then precisely defined to trap water droplets, perform micro batch simultaneous chemical reactions and even multiple incubators for small volume bioassays in a reticulated silicone elastomer matrix.

4.1.2. Emb3D/ODP: Embedded 3D printing/ Omnidirectional printing

The ODP/Emb3D technique, already described for negative passive Freeform (paragraph 3.1.1), was transposed to silicone elastomer matrices applications. A really complete study about impact of fluid deformation and rheological instabilities around the moving tip was performed by Freeform 3D printing of F127 within silicone elastomer [33] (**Figure 4B**). The authors determined that relationships do exist between the dimensions of the yielded region and the rheological properties of the matrix materials, impacting then the printing parameters.
The method was then applied to the production of strain sensors and pneumatic actuators within highly conformal and extensible elastomeric matrices [14,42] (**Figure 4C**). In these cases, conducting carbon grease and ionogel inks were patterned within silicone elastomer matrix. The curing by polyaddition of the silicone matrix thus led to functional and stretchable strain sensors with proprioceptive, haptic and thermoceptive sensing for human-machine interface applications [14,42]. The ODP/Emb3D technique was further used in voice biomechanics where silicone vocal folds were printed [48]. Made of multiple layers of soft silicone, down to 160 µm in resolution, the vocal folds demonstrated phonation with vibration characteristics similar to the native human vocal folds.

4.1.3. Solid object sculpting

In this method, similar to the one proposed by Compaan *et al.* [35] (paragraph 3.1.2), multi-internal surfaces structures composed of a crosslinked blend of Carbopol® were generated [47] (**Figure 4D**). To do so, photocurable acrylamide and poly(ethylene glycol) diacrylate were blended with Carbopol® microgel and use as a Freeform support matrix. Then, a silicone oil-based ink was used to Freeform the external contours of the final object. Once the printing completed, the Carbopol® blend was UV cured and the crosslinked silicone oil used as a releasing layer for organ pre-operative surgery training. Similarly, Tejo-Otero *et al.* [49] proposed a variation of the FRESH using another thermoreversible matrix (paragraph 5.1.4) to perform solid object sculpting. A silicone ink was

Freeform 3D printed to produce hollow pre-operative surgery training liver phantoms (with 0 and 10% infill) within an optimized F127 matrix rheology [50]. After the silicone curing through hydrosilylation, tissue-mimicking liver phantoms were retrieved by liquefying the matrix through cooling and a silicone coating was added to make the construct waterproof. With the entrapment of the matrix inside, the printed liver showed comparable viscoelastic properties mimicking the soft liver tissue. In the present review, these approaches were named solid object sculpting and classified in the passive null class, even if some part of the matrix is being removed after printing.

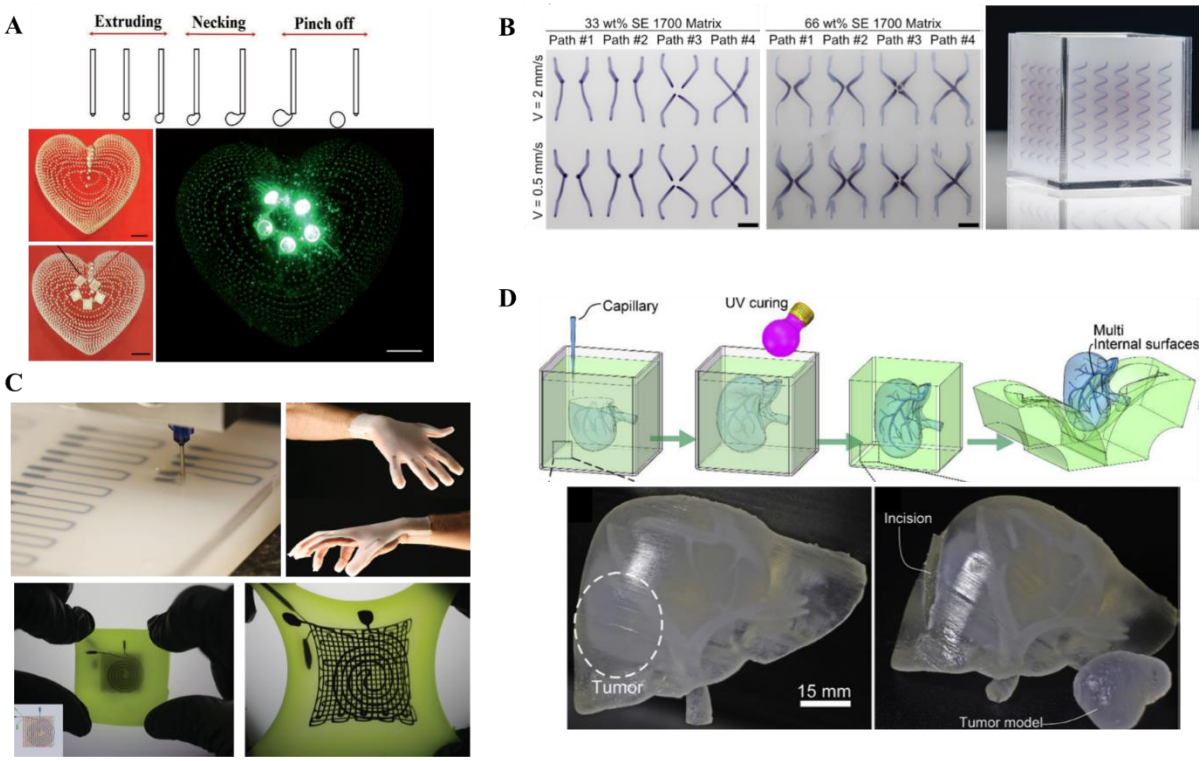

Figure 4. Overview of the printed structures using passive null Freeform 3D printing**.** (A) Principle of droplet generation in the embedded droplet printing technique. Heart-shaped construct composed of metal Gallium-Indium alloy droplets suspended in Carbopol®. Scale bars 10 cm. Adapted with permission from *[43]*. Copyright (2017) WILEY-VCH. (B) Emb3d/ODP printing of F127 solution within PDMS for the study of fluid deformation fields during Freeform 3D printing. Change of pattern morphology due to the increase of yield stress of the PDMS matrix (left). Example of Freeform construct (right). Scale bars 3 mm. Adapted with permission from *[33]*. Copyright 2018, ACS. (C) Emb3D/ODP printing of conducting carbon grease for stretchable strain sensors embedded in a cured PDMS structure. Glove and three-layer strain and pressure sensor at rest and stretched. Adapted with permission from *[14]*. Copyright 2014, WILEY-VCH. (D) Scheme of the solid object sculpting in crosslinkable Carbopol® blend (top). By patterning hollow paths using silicone oil, the final construct contains the crosslinked Carbopol® matrix. Liver anatomical model containing a tumor and its removal by incision. Adapted with permission from *[47]*. Copyright 2020, ELSEVIER.

4.2. Active null Freeform 3D printing

4.2.1. FREAL: Freeform reconfigurable embedded all-liquid

Freeform reconfigurable embedded all-liquid microcontructs (FREAL) is based on an aqueous two-phase systems [44] composed of immiscible hydrophilic polymers ink and matrix. At the interface of the ink solution (Polyvinyl alcohol (PVA) Polyacrylamide (PAAM), Poly(acrylic acid) (PAA) or Dextran) and the PEO matrix, low interfacial tension is generated (down to 0.04 $mN.m^{-1}$), limiting deformation and instabilities of the printed liquid structures (**Figure 5A**). An interfacial membrane locks then the construct via hydrogen bounds, stabilizing the printed structures over long-time scales. The obtained all-liquid microconstructs exhibit resolution down to 200 µm and shall have applications for *in vitro* tissue-on-chip or tissue regeneration. The stability of the final object depends on the interaction between the matrix and the ink, classifying then FREAL in the active null class.

4.2.2. GHost-writing

GHost-writing (paragraph 3.2.2) relies on rapid supramolecular non-covalent reversible bonds between molecules present within the matrix but also contained within the ink [41]. The technique, initially developed as an active negative Freeform method was further used for active null printing leading to the encapsulation of complex shapes of modified hyaluronic acid (adamantane or cyclodextrin) within modified hyaluronic acid matrix without further crosslinking. Stable complex shapes such as spirals or material pockets were thus obtained, opening the path to multimaterial Freeform 3D printing. Another technique exploiting ion-ligand non-covalent reversible bonds [51] in both ink and matrix (paragraph 5.2.4) encapsulated cell adhesive peptides to recreate the biochemical properties of the native tissues (**Figure 5B**). The acrylamide-functionalized ink and matrix were then stabilized through UV photocrosslinking.

4.2.3. Reconfigurable printed liquids

As an evolution of the FREAL method, Forth *et al.* [46] developed an all-liquid technique using amino-modified silicone oil in which an aqueous ink, composed of a solution of 20 nm carboxylic acid functionalized silica nanoparticles, was Freeform 3D printed (**Figure 5C**). During printing, amino and carboxylic functions interact electrostatically, thus stabilizing the interface. The final objects, composed of 10 to 1000 µm size features suspended in a silicone oil matrix, were expected to be indefinitely stable and have potential applications in encapsulation of cells or active chemicals, chemical synthesis and all-liquid electronics.

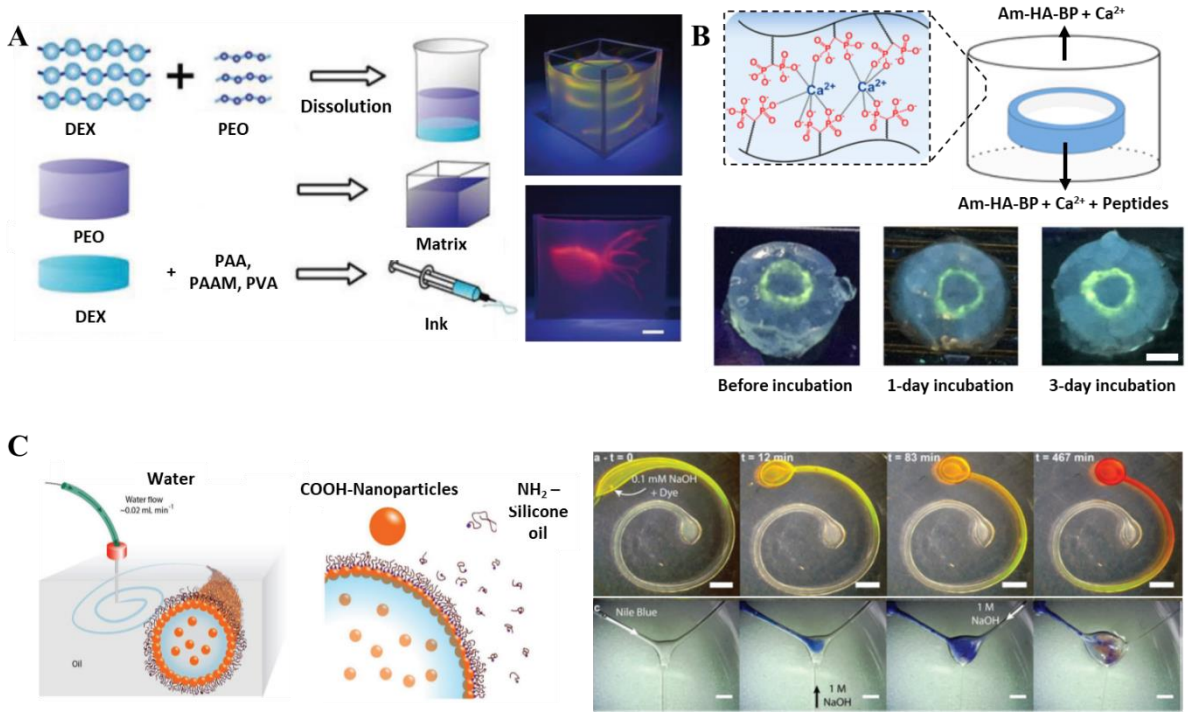

Figure 5. Overview of the printed structures in active null Freeform 3D printing. (A) Principle of aqueous two-phase system for FREAL. All liquid channels stabilized through hydrogen bounds. Scale bar 10 mm. Adapted with permission from *[44]*. Copyright 2019, WILEY-VCH. (B) Principle of ion-ligand non-covalent reversible bonds of acrylamide and bisphosphonate functionalized-hyaluronic acid (Am-HA-BP) and calcium cation matrix and ink. Fluorescent living cells adherent to peptides modified ink. Scale bar 2 mm. Adapted with permission from *[51]*. Copyright 2017, ACS. (C) Extrusion of an aqueous ink composed of 20 nm carboxylic acid functionalized silica particles. The extruded nanoparticles react with amino-functionalized silicone oil, stabilizing the construct (top). Demonstration of microchannel Freeform 3D printing through perfusion of multiple solutions. Scale bars 3 mm. Adapted with permission from *[46]*. Copyright 2018, WILEY-VCH.

5. Positive Freeform 3D printing

Positive Freeform 3D printing is probably the most known and widespread Freeform technique. The final product is always composed of the ink after elimination of the supporting matrix which allows to maintain the printing shape with high fidelity until hardening. This ink solidification can be triggered through various methods such as temperature change, irradiation or soft chemistry (chelation, enzymatic reaction). In the frame of Active positive Freeform 3D printing, this solidification is triggered *in-situ* by the matrix stabilizing the construct from fluid instabilities and gravity [10,34].

5.1. Passive positive Freeform 3D printing

5.1.1. FRE/PTG: Freeform Reversible Embedding/Printing-Then-Gelation

Freeform Reversible Embedding (FRE) [11,16] and Printing-Then-Gelation (PTG) techniques [17] were here included in the same class which cover multiple Freeform 3D printing techniques based on microgel matrices. FRE, proposed by Hinton and coworkers [11], a more general term of FRESH (paragraph 5.1.4) [16], was first focused on silicone extrusion within a hydrophilic matrix composed of Carbopol® microgels. This commercially available polymer of poly(acrylic acid) is widely used as a matrix in other Freeform techniques (**Table 1**) and exhibits yield stress behavior [15] at particle volume fraction in solution of 0.58. At this ratio, the microgel was proven to be in a random loose packing conformation bringing yield stress and shear thinning behavior. Once the printing completed and the silicone cured, the Carbopol® matrix was liquefied using standard aqueous buffer, and complex parts such as helices and tubes mimicking vascularization were recovered. Interestingly, in order to further optimize FRE, multiple studies have been using machine learning [52,53] to determine printing conditions allowing faster prints while keeping high print fidelity. Meanwhile, other studies focused on high speed printing and the occurring instabilities [12,32,54,55]. In the present review, all these approaches were named FRE and classified in the passive positive class.

In term of application, the medical field is the most impacted by the FRE techniques. Examples of such healthcare applications are wearable patient-specific oximeters [56], composed of printed silicone elastomer used to produce soft electronics (**Figure 6A**). An adaptation of the FRE to handle biopolymers was used to generate vascular structures from coaxial printing [57] or with interpenetrating network hydrogels [58] and recombinant human tropoelastin [59]. Living cells extruded in microgel were also studied for tumor engineering [60] while inks composed of collagen low-concentration was used for intestine tissue engineering [61].

In numerous biological applications, including bioprinting, alginate is one of the major ink components, which shall be consolidated through calcium chelation. Nevertheless, Carbopol® is known to react with multivalent cations, leading to a shrinkage of the microgels and then a loss of its yield stress behavior. Direct printing of alginate within calcium loaded Carbopol® is then not a viable option. To cope with this issue, Printing-Then-Gelation (PTG) [62] was developed based on the use of a special ink composed of alginate and gelatin. Here, once Freeform 3D printed, the structure is cooled down to be solidified and removed from the Carbopol® matrix, gelatin holding the structure. The object can then be consolidated through gelation in a calcium bath before removing the sacrificial gelatin at 37°C.

PTG developments were also performed using other matrices such as yield stress aqueous Laponite® nanoclay colloidal suspensions or Gellan fluid microgel [17]. Interesting results were here obtained for the Freeform fabrication of biological or synthetic polymers (alginate, gelatin, polyethylene glycol diacrylate (PEGDA)), but also for the study of fluid flow deformation around the tip and printability studies [63–65].
Other microgel matrices examples are a suspension of alginate microparticles in a solution of xanthan gum for engineering cardiac and vascular patches [66] but also a microgel of lightly crosslinked polyacrylamide for intestine tissue engineering [61].

5.1.1.a. AAFB: Aspiration-Assisted Freeform Bioprinting

A new technique, not extrusion-based, was developed by Ayan and coworkers [26] and termed Aspiration-Assisted Freeform Bioprinting (AAFB) of cell spheroids for bone and cartilage tissue engineering. In this technique, cell spheroids in a cell culture media compartment are gently aspirated and precisely deposited within a Carbopol® or alginate microgel buffered with cell culture media. Constructs such as a double helix and tube made of 150-400 µm spheroids demonstrated stability after 28 days of culture. This technique is a powerful approach to generate anatomically relevant tissues and organs. Similarly Daly *et al.* [67] used the AAFB technique within a self-healing modified hyaluronic acid matrix (adamantane and cyclodextrin, see paragraph 3.2.2) for cardiac tissue engineering and drug screening applications.

5.1.1.b. CLASS: Constructs laid in agarose slurry suspension

Constructs Laid in Agarose Slurry Suspension (CLASS) [68] is a type of the FRESH technique (paragraph 5.1.4) that uses agarose microparticles suspension , as matrix for bioprinting. In contrast with FRESH, in CLASS, the matrix is produced by blending a cold agarose hydrogel then centrifugated to produce an agarose microparticle suspension. Agarose microparticle suspension was found to be easier to prepare, was less sensitive to blend time and to the printing temperature. This was attributed to the higher melting temperature of the agarose (93 to 96°C), allowing the culture of printed constructs at body temperature without losing its suspending properties. was demonstrated by an extended culture over 11 days of cell-laden collagen and gelatin methacrylate (GelMA) constructs kept in the agarose matrix, crosslinked by temperature and UV respectively, showing cell proliferation and retaining their original shapes.

5.1.1.c. DF3DP: direct freeform 3D printing

In an eco-friendly approach and to avoid wasting not reusable Carbopol® [69], Tan *et al.* [20] elaborated a reusable and recyclable green matrix based on alginate in which silicone ink was Freeform 3D printed to produce wearable silicone elastomer membranes [20,69]. The authors named their FRE method Direct Freeform 3D printing Process (DF3DP). The matrix consists of spherical microgels of chelated alginate produced by extrusion dripping. An alginate solution was extruded on a vibrating unit at 6000 Hz causing the filament to break into droplets, chelated in a calcium solution, then dispersed mechanically and electrostatically.
To ensure the reusability [69], the spherical alginate microgel underwent mild post-processing conditions (post curing at 75°C during 24h) (**Figure 6B**). The rheological deviations, consequences of this post-process, were found to be related to water evaporation. The authors cope this issue by adding glycerol as humectant in the matrix

formulation and a rehydration step in NaCl solution (0.45 wt% or 0.9 wt%) followed by a recovery in calcium cations bath.

Jeon and coworkers [70] modified the DF3DP technique by using UV-crosslinkable oxidized and methacrylated alginate for cell-only extrusion to promote the self-assembly of tissue. The matrix is crosslinked to retain its shape, which reduces its degradability and maintains the cell-only construct for culture up to 4 weeks. After maturation, the complex constructs such as human bones and ear models were retrieved from the matrix through agitation.

5.1.1.d. IBPC: In-bath print and cure

In a technique termed In-Bath Print and Cure (IBPC), Mahmoudi and coworkers [71] used an aqueous colloidal suspension of Laponite® similarly to PTG (paragraph 5.1.1), as a matrix for printing thermosets. Laponite® is a synthetic smectite nanoclay and is in the form of nanoscale platelets with high aspect ratio (approximately 1 nm thick and 25 nm in diameter). In aqueous solutions they disperse to form colloidal suspensions. When dispersed, ions dissociate from each platelet's surface electrostatically stabilizing the individual platelets in a structure bringing yield stress and thixotropic behavior [63,72]. The IBPC technique enabled the extrusion of epoxy and a carbon fiber reinforced composite epoxy. Once the printing completed and the thermosets thermally cured, the complex parts such as helical coils and fan were recovered and rinsed with water. The reinforced composite epoxy showed carbon fiber alignment along the filament axis and isotropic mechanical properties which open opportunities for composite Freeform 3D printing.

5.1.1.e. SLAM: Suspended layer additive manufacturing

The Suspended Layer Additive Manufacturing (SLAM) technique was proposed by Moxon *et al*. [73] and is based on an original preparation of matrices named sheared gels. In this approach, a self-healing and non-thixotropic matrix is produced through the introduction of shear during the sol-gel transition of agarose hydrogel, producing entangled hair-like and irregular microparticles. The weak entanglement between the irregular agarose microparticles can be disturbed by shear, allowing these materials to be used as Freeform 3D printing matrices. In term of applications, SLAM focuses on regenerative medicine. Examples of such applications are cartilage and bone reconstruction using gellan gum combined with hydroxyapatite or Laponite® [74]. composite biopolymer structures (collagen/gellan and collagen/alginate) mimicking soft tissue structures [75] and human platelet lysate hydrogel ink to recapitulate anatomical hierarchical fibrous structures [76]. The obtained constructs were retrieved after solidification through calcium chelation for both gellan gum, by temperature increase for collagen and using thrombin for the fibrin enzymatic polymerization in the platelet lysate.

5.1.2. 3D plotting

3D plotting technique developed by Landers and Mülhaupt [77] is based on the extrusion within liquid, non-yield stress matrices. To do so, the density of ink and matrix are matched to prevent collapse of the 3D printed objects. Detailed structures can be achieved with a resolution down to 200 µm. Typical examples are silicone elastomer scaffolds printed in water for biomedical applications [77], but also agar scaffolds printed in fluid gelatin solution subsequently coated to promote cell adhesion and cell growth for tissue engineering applications [78].

5.1.3. BATE: bioprinting-assisted tissue emergence

Similar to the works of Jeon *et al.* (paragraph 5.1.1.c), Bioprinting-Assisted Tissue Emergence (BATE) [79] exploits the self-assembly of cells to produce centimeter-scale detailed and relevant biological structures for tissue engineering. The ink contains only human cells and is extruded in cell culture matrices (Matrigel®, collagen, methylcellulose). After maturation and cell self-assembly, human colon tubes, connective tissue and a vein recapitulating native tissue functionality and shape were obtained. As an example, the self-assembled human vein was perfusable and when further adding growth factors, capillaries developed with diameters lower than 50 µm. Then the matrices were enzymatically degraded to release the prints. The technique was proposed as a solution creating complex anatomically relevant tissues while reducing printing time.

5.1.4. FRESH: Freeform reversible embedding of suspended hydrogels

FRESH, was first introduced by Hinton and coworkers [18] for active positive Freeform of biopolymer extrusion (alginate, fibrin and collagen) within a hydrophilic matrix composed of gelatin microparticles suspension produced by blending a gelatin hydrogel then centrifuged. Once the printing completed and biopolymers consolidated, the matrix was liquefied by temperature increase at 37°C and complex biological parts such as human femur and coronary arterial tree were recovered. FRESH is defined by [16,18] 1) the use of a yield stress matrix, 2) compatibility with multiple aqueous phase for multiple gelation mechanisms of the ink, 3) controllable and non-destructive liquefaction of the matrix for print release under biologically compatible conditions. FRESH, as FRE, is widely used principle in other Freeform techniques (**Table 1**).

In the frame of passive positive Freeform applications, FRESH focuses on healthcare. Examples of such applications are the synthesis of nano hydroxyapatite for bone reconstruction [80,81], biocompatible oxidized alginate microgel-based ink for cryopreserving cells [82] or generation of tumor organoids for drug screening [83]. Other works were performed on bioprinting miniaturized beating heart [84], *in-vivo* recellularization and simulation of collagen printed heart valves [85,86] and muscle reconstruction through coaxial printing [87].

FRESH developments were also performed using other matrices exploiting the third property of FRESH (controllable and non-destructive liquefaction of the matrix) by using other thermoreversible matrices such as Pluronic® F-127. Consequently, in this review, these other techniques are also named FRESH. In these studies, silicone ink was Freeform printed to produce organ pre-operative surgery training through 6-axis printing within an optimized matrix rheology [50] (**Figure 6C**). Applications were also demonstrated for the printing of magnetic helical coil actuators [88].

5.1.5. EDIW: embedded direct ink writing

Embedded Direct Ink Writing (EDIW) was proposed by Huang *et al.* [89] who used vegetable oil and hydrophobic fumed silica as a hydrophobic matrix for the printing of silicone and polymer inks (Poly(vinyl butyral), PEO) filled with ceramic or metal powders. The matrix, composed of a suspension of fumed silica nanoparticles, exhibits yield stress behavior thanks to the assembly of the particles into a percolated network structure. Once printing completed, the ink was cured and pyrolized and complex ceramic and metallic parts such as helical coils were recovered and rinsed with water or ethanol [90]. Other authors published with a similar approach but using mineral oil instead of fumed silica nanoparticles suspension. They extended then the EDIW to the extrusion of commercially available

hydrophobic polymers (silicone elastomer, photocrosslinked resin, conductive composite epoxy) [91] and polymer-derived silicon oxycarbide ceramic [90]. Interestingly, the authors shown that these hydrophobic matrices exhibited high temperature stability up to 160°C, useful for effective polymer curing. Another positive point of using these hydrophobic matrices was the reduction of surface tension, leading to higher stability of the extruded filament [34].

5.1.6. EIW: embedded ink writing

Karyappa *et al.* [92] proposed the Embedded Ink Writing (EIW) as a tool to produce planar microconstructs for microfluidics and wearable devices (**Figure 6D**). To do so, silicone is extruded on a polystyrene (PS) substrate in an immiscible polar liquid matrix (methanol, ethanol, and isopropanol). The high interfacial tension locks the liquid silicone patterns until thermal curing is completed. Then, the liquid matrix is removed by evaporation, leaving high resolution (65 µm) stable planar smooth microconstructs.

5.1.7. Emulsion glass

In an eco-friendly approach, Hu *et al.* [93] elaborated a reusable and recyclable matrix using a silicone oil-in-water emulsion termed emulsion glass. The matrix consists of jammed silicone oil droplets at high volume fraction (over 85%) in an aqueous solution of sodium dodecyl sulfate surfactant. According to the authors, this matrix shall be termed emulsion glass since it has an amorphous structure and is kinetically stable over long time scales. Thermal and UV-curing silicone inks were Freeform 3D printed to produce freestanding helical coils. The thermal-curing process was performed at 100°C. The retrieved objects were then rinsed with water. The matrix was found to be stable after the ink curing processes, no photodegradation nor thermal degradation was observed, making the matrix reusable (at least 6 times).

5.1.8. Freeform in a supporting viscous liquid

As an evolution of the 3D plotting technique (see section 5.1.2), Uchida and Onoe [94] performed Freeform in a supporting viscous liquid of carboxymethyl cellulose solution for the production of 4D thermo-responsive hydrogels. The ink was composed of a blend of non-responsive material (acrylamide (AAM)), thermo-responsive material (N-isopropylacrylamide (NIPAM)) and sodium alginate. After UV polymerization, the obtained 4D structures exhibited shape changing response, due to anisotropic deformation, upon cyclic thermal stimuli. In their original work, authors named their technique Direct Ink Writing in a supporting viscous liquid, which was renamed in this review as Freeform in a supporting viscous liquid and then classified in the passive positive class.

5.1.9. Micro-organogel support matrix

O'Bryan *et al*. [34] developed an oil-based microgel matrix, referred as micro-organogel and based on the self-assembly of block copolymers for printing UV-curing silicone. In this approach, the nonpolar matrix is produced and tuned through the self-assembly of diblock copolymers of Polystyrene-block ethylene/propylene (SEP) and triblock copolymers of Polystyrene-block ethylene/butylene-block-polystyrene (SEBS) solubilized in mineral oil. When mixed, copolymers both self-assemble into nanometric glassy polystyrene cores, connected by the ethylene/butylene blocks of SEBS, yielding a macroscopic network.

The key advantage using this approach is the low interfacial tension of the developed matrix, enabling high precision (50 µm diameter filaments) Freeform printing. After printing, recovered complex parts, such as pumps and a model of human trachea, were washed with surfactants and rinsed with ethanol. In a phonation modelling application, Romero *et al.* [95] used this matrix to produce self-oscillating vocal folds models [95] for human voice research. The models were able to oscillate at a similar amplitude and frequency to human ones.

5.1.10. SMAP: Solid Matrix Assisted 3D Printing

An emerging field for the Freeform 3D printing is the use of matrices composed of solid particles powders with adapted flowability [96]. Sin and coworkers [97] developed a technique termed Solid Matrix-Assisted 3D Printing (SMAP) for printing bacterial cellulose (BC) hydrogels within poly(tetrafluoro ethylene) (PTFE) particles powder (**Figure 6E**). BC is a polysaccharide synthesized by aerobic biosynthesis widely used in biomedical applications thanks to its mechanical properties and high biocompatibility. In the SMAP technique, BC is *in situ* biosynthesized within the hydrogel ink through aerobic biosynthesis of cellulose nanofiber by an active bacteria thanks to the PTFE matrix oxygen permeability. In contrast with usual fluid matrices where fluid rheology dominates the process, here, particle powder flowability is the main impacting factor, driving Rayleigh-Plateau-like instabilities and crevasse generation. Post printing, the complex objects such as blood vessel models were kept within the solid matrix for incubation during 7 days. The hydrophobic PTFE powder is immiscible with the hydrogel ink, classifying then SMAP in the passive positive class.

5.1.11. Submerged 3D bioprinting

With the growth of bioprinting technologies, some difficulties arise for bioprinted structures that needs nutriment or oxygenation during printing or culture. As an alternative, Campos *et al.* [98] proposed the submerged 3D bioprinting technique by using fluorocarbon (perfluorotributylamine) as a fluid matrix, similar to the 3D plotting technique (paragraph 5.1.2). Fluorocarbons are high-density and biocompatible nonpolar fluids with high dioxygen and carbon dioxide diffusion. Using the density matching and high surface tension (contact angle up to 70°), agarose constructs with smooth surfaces were obtained. Cylindrical acellular agarose constructs were found to be stable over 6 months while cellular constructs proliferated and remained viable after 21 days in culture within the fluorocarbon matrix.

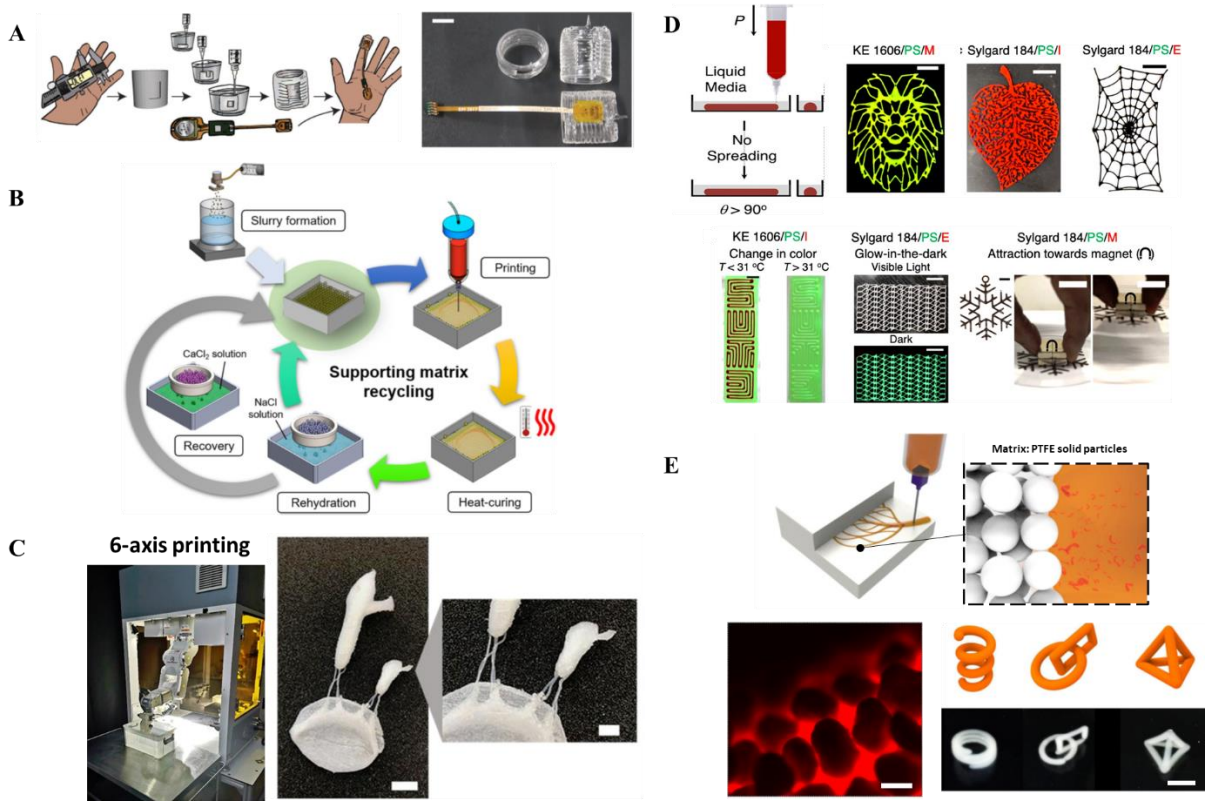

Figure 6. Overview of the printed structures in passive positive Freeform 3D printing. (A) FRE of patient-specific flexible oximeter with integrated flexible printed circuit. The device performs long-term monitoring while being tightly attached on the patient. Scale bar 10 mm. Adapted with permission from *[56]*. Copyright 2020, WILEY-VCH. (B) Optimal process cycle for large-scale FRE printing by using a recyclable alginate microparticulate matrix. After Freeform 3D printing and curing, the matrix can be rehydrated or immersed in a calcium solution to maintain the optimal rheological properties required for the technique. Adapted with permission from *[69]*. Copyright 2020, SPRINGER. (C) FRESH 3D printing of a complex anatomical PDMS structure (human mitral valve, cordae tendineae and papillary muscles for surgical training. This was achieved by using a 6-axis printer within a thermoreversible and reusable PEG/F127 matrix. Scale bars 10 mm and 5 mm (closer view). Adapted with permission from *[50]*. Copyright 2021, LANGMUIR. (D) Principle of EIW of silicon within fluid alcohol. The high interfacial tension between matrix and ink prevents construct's sag. Examples of constructs for microfluidic devices or soft wearable functional tissues (thermoresponsive, fluorescent and magnetic). Adapted with permission from *[92]*. Copyright 2020, ACS. (E) Principle of SMAP printing (top) using poly(tetrafluoro ethylene) (PTFE) particles as matrix. PTFE particles bind at the surface of the filament of bacterial cellulose hydrogel ink (bottom left). Examples of Freeformed shapes using the SMAP technique (bottom right). Scale bars 100 µm (bottom left) and 10 mm (bottom right). Adapted with permission from *[97]*. Copyright 2019, NATURE.

5.2. Active positive Freeform 3D printing.

5.2.1. FRE/PTG: Freeform Reversible Embedding/Printing-Then-Gelation

As in section 5.1.1, Freeform Reversible Embedding (FRE) [11,16] and Printing-Then-Gelation system [17] were here included in the same class. To perform active Freeform, calcium-loaded xanthan gum, previously used in

active negative Freeform (see section 3.2.3), was used for the Freeform 3D printing of alginate inks. The calcium-loaded matrix enabled the chelation of the extruded alginate directly during printing. Once the print completed, complex parts such as blood vessels were retrieved and rinsed with water. Bioprinting was also performed using this technique by encapsulating cells in the alginate ink and constructs showed viability over 7 days of culture.
Active Freeform printing using PTG were performed using matrices such as yield stress gellan microgel and aqueous Laponite® nanoclay colloidal suspensions [17] for medical applications and tissue engineering. Examples of such healthcare applications are supporting constructs composed of gelatin, alginate or cell-laden gellan hydrogel *in-situ* crosslinked with transglutaminase and chelated with calcium ions, respectively [17,63].
In a similar study, silk fibroin was Freeform printed as cell culture supports for anisotropic neuromuscular junction tissue engineering within a polyethylene glycol (PEG)-nanoclay suspension matrix [21,99]. The silk fibroin ink was crosslinked *in situ* with the presence of PEG contained in the nanoclaymatrix then rinsed with aqueous buffer. The obtained silk structures were stable enough to allow a cell culture of 4 weeks.
The techniques that will be presented in the following paragraphs are considered as FRE-PTG subclasses since they all use microgel-based matrices.

5.2.1.a. CLASS: Constructs laid in agarose slurry suspension

Constructs Laid in Agarose Slurry Suspension (CLASS) [68] (paragraph 5.1.1.b) was further used for active positive printing for cell-laden alginate constructs using a calcium-loaded agarose microparticle suspension matrix. Printability of the ink was asserted through pressure and moving speed variations. The alginate-calcium layer was stable enough allowing the patterning of complex shapes such as honeycomb and helixes constructs.

5.2.1.b. Embedded droplet printing

As presented before, Nelson *et al.* [45] continued to use the embedded droplet printing for manufacturing crystalized spherical particles within Carbopol®. The obtained powders can be used in pharmaceutical applications for tablet production. The authors used an anti-solvent crystallization approach where ethyl acetate droplets containing a blend of active pharmaceutical ingredient and excipient were printed. The ethyl acetate diffuses in the matrix triggering the spherical crystallization of the pharmaceutical product (**Figure 7A**). The matrix is then liquefied with aqueous buffer yielding a pharmaceutical powder with improved flowability.

5.2.1.c. FPP: Freeform Polymer Precipitation

Current Freeform 3D printing technologies are not compatible with thermoplastic material requiring high temperatures extrusion. To cope with this issue, Freeform Polymer Precipitation (FPP) [19] was developed by Karyappa and colleagues, exploiting the anti-solvent precipitation approach. By extruding thermoplastics solubilized in adapted solvents, these latter precipitate when in contact with the aqueous Carbopol® matrix. Tuning of the solvent solubility in Carbopol®, enabled tuning the objects porosity through the interaction between ink and matrix (active Freeform). 14 different thermoplastics were thus processed through FPP (such as PS, thermoplastic polyurethane, acrylonitrile-butadiene-styrene (ABS), etc.). Objects such as helical coils were retrieved after matrix liquefaction.

5.2.1.d. Multifunctional granular composite matrix

Heo *et al.* [100] developed a matrix composed of gelatin microparticles suspended in an oxidized alginate solution for the Freeform printing of carbohydrazide-modified gelatin. During extrusion, the carbohydrazide-modified gelatin reacts with oxidized alginate microparticles forming imine bonds via Schiff-base reaction, leading to a composite and highly biocompatible hydrogel. The chemical reaction allowed high structural stability and cell viability after matrix removal and rinsing with aqueous buffer, yielding complex meshed tubes, spheres and humerus model (**Figure 7B**).

5.2.2. FRESH: Freeform reversible embedding of suspended hydrogels

In the frame of active positive Freeform applications, FRESH [18] expanded in bioprinting and tissue engineering fields and enabled the Freeform printing of relevant biological structures and materials. This includes a human heart model (full-size) made of alginate [101], a collagen based beating and heart model left ventricle (**Figure 7C**) [102], some collagen-alginate corneal tissue substitutes [103], 3D culture of neuroblastoma cells in sodium alginate for cancer research [104,105] but also carrot-alginate constructs for food printing [106]. These constructs were manufactured thanks to the versatility of the gelatin microparticle suspension matrix which may support numerous consolidation reactions thanks to the advances in biorthogonal crosslinking [107,108]. As an example, the use of calcium-loaded matrix enables the chelation of alginate [101,104,109], the collagen bioink self-assembles through rapid pH changes or by temperature increase [102,103] or fibrinogen is enzymatically converted *in-situ* by the thrombin added in the matrix [110]. Advances were also performed in the development of printers, to spread tissue engineering via low-cost devices [111–114] and FRESH optimization using machine learning [104,111]. As mentioned before (paragraph 5.1.4), number of researchers adopted FRESH 3D printing technique by using thermo-reversible matrices such as F127 or F127-Laponite micelle suspensions to support alginate extrusion [115,116] or cell-laden constructs for tissue engineering [72], respectively.

The following methods, even if not named clearly FRESH by the authors, use gelatin microparticles suspension as matrix, and were herein grouped with the FRESH techniques.

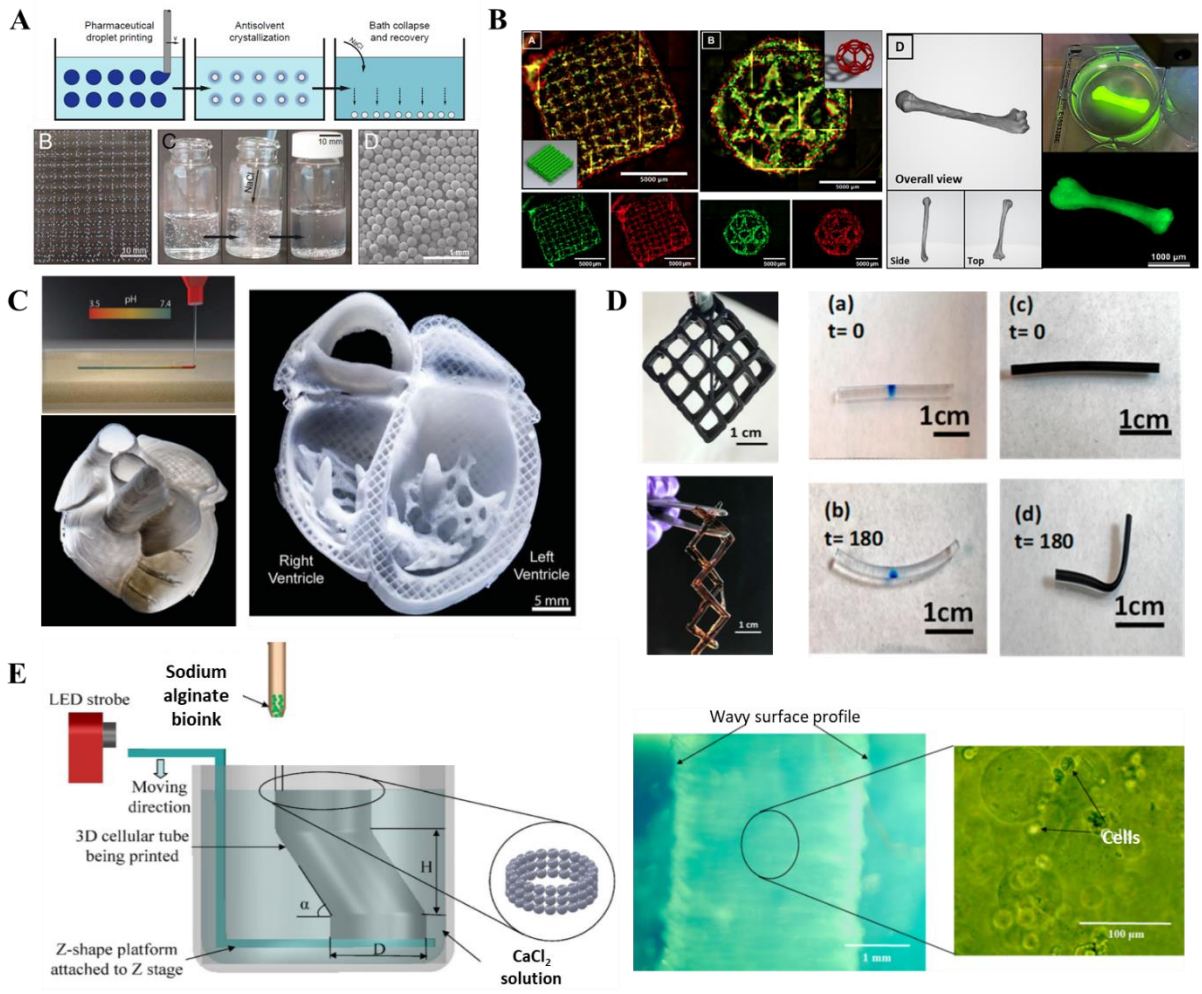

Figure 7. Overview of the printed structures in active positive Freeform 3D printing. (A) Principle of anti-solvent crystallization of pharmaceutical compounds using the embedded droplet printing (top). The solution (ethyl acetate) diffuses in the Carbopol® matrix triggering the spherical crystallization of the drug (bottom). Scale bars 10 mm and 1 mm (closer view of particles). Adapted with permission from *[45]*. Copyright 2020, PNAS. (B) Cell-laden constructs of composite hydrogel under fluorescence microscopy. The carbohydrazide-modified gelatin ink reacts during extrusion with the oxidized alginate matrix to form a composite hydrogel. Adapted with permission from *[100]*. Copyright 2020, ACS. (C) Collagen organ-scale printed human heart using FRESH technique where acidic collagen ink gelled through rapid pH change. Adapted with permission from *[102]*. Copyright 2019, AAAS. (D) Constructs of F127 graphene oxide and multiwalled carbon nanotubes (CNT) composites formed in-situ during the catalytically initiated gel-in-gel printing. Volume change of constructs through photothermal effect: pure F127 constructs showed low response (middle) whereas F127-CNT ones showed high shrinkage (right). Adapted with permission from *[117]*. Copyright 2017, ACS. (E) Platform-assisted 3D inkjet bioprinting of a complex tube. The ink rapidly solidifies through chelation by the calcium solution matrix and allowed cell attachment. Adapted with permission from *[25]*. Copyright 2012, WILEY-VCH.

5.2.2.a. Catalytically initiated gel-in-gel printing

Basu *et al.* [117] proposed the catalytically initiated gel-in-gel printing of cross-linkable F127-dimethacrylate, curing in the presence of free radicals from ammonium persulfate and catalysed by the presence of tetramethylethylenediamine within the F127 matrix. Once the object consolidated and the matrix liquefied by temperature decrease, constructs of cross-linked F127 were retrieved as well as conductive composites of F127-multiwalled carbon nanotubes, useful for infrared photoresponsive actuators (**Figure 7D**).

5.2.2.b. COBICS: ceramic omnidirectional bioprinting in cell-suspensions

Condensation of Ceramic Omnidirectional Bioprinting In Cell-Suspensions (COBICS) exploits the rapid solidification of calcium phosphate in aqueous environments for bone tissue engineering. This is one seldom example of ceramic processing using Freeform 3D printing [118]. Calcium phosphate is a material mimicking porous bone composition and mechanical properties. When extruded and solidified within a gelatin matrix seeded with cells, hierarchical porous structures of ceramic nanocrystals were generated without the need of high temperature sintering. Cells found in the matrix were differentiating at the surface of the porous construct, bringing opportunities for tissue engineering applications.

5.2.2.c. Freeze-FRESH

An original combination of FRESH 3D printing and freeze-casting, followed by lyophilization [119] and named Freeze-FRESH, has been proposed to produce porous alginate/hyaluronic acid scaffolds for breast cancer studies and recently optimized for collagen extrusion [120]. The innovation here was to leverage the difficulties of hierarchical pore production from freeze-casting and lyophilisation processes, by patterning macroscale pores during printing. The alginate/hyaluronic acid ink was extruded and chelated within a calcium-loaded gelatin matrix and then the overall was freeze-casted in the gelatin matrix. After the freeze-casting, the matrix is melted at 37°C following the complete crosslinking of the constructs in a calcium solution and are ready for cell culture . The constructs underwent freezing down to -20°C or -80°C, leading to an average 60% porosity characterized by 300 µm diameter pores. The process resulted in a 50% shrinkage of the constructs during the post-printing freezing treatment. Freeze-FRESH enabled the production of porous scaffolds promoting breast cancer cell adhesion and clusters formation, improving breast cancer growth *in vitro*.

5.2.2.d. In-situ precipitation coupled FRESH 3D printing

Another inorganic material Freeform 3D printing was here developed. It consists in the *in-situ* precipitation of calcium cations and phosphate anions into calcium phosphate nanoparticles for bone tissue engineering [121]. A photocurable ink composed of alginate and bisphosphonate functionalized hyaluronic acid (HA-BP) was extruded within a calcium-loaded gelatin matrix. During extrusion, alginate consolidates via chelation and calcium phosphate nanoparticles nucleates, starting from the functional groups of the HA-BP. After UV triggered reticulation, a uniform calcium phosphate nanoparticle coating was obtained with spherical nanoparticles of 60 nm, enhancing mechanical properties and cell attachment. Constructs such as scaffolds with gradients of calcium phosphate nanoparticle concentrations were obtained bringing opportunities for various biomedical applications.

5.2.2.e. TMF bioprinting: Triggered Micropore-Forming bioprinting

Proposed by Bao and coworkers [122], the Triggered Micropore-Forming (TMF) bioprinting technique is based on *in-situ* micropore formation induced by phase separation and triggered pH change. A chitosan solution ink reacts with a sodium bicarbonate-loaded gelatin slurry and separates into bicontinuous microphases. PEG was added to the porous hydrogel to tune viscoelastic properties through hydrogel bonding with chitosan. The obtained bicontinuous water-chitosan microphase with 20 µm average size of micropores, presented concentrated regions of chitosan, stiffening global the printed construct. The microporous hydrogel was demonstrated to promote cellular activity and the versatility of this technique was evaluated through the printing of a cell-laden vocal fold and breast cancer models.

5.2.3. 3D plotting

Dubbin and coworkers [123] developed a novel bioink based on the Mixing-Induced Two-Composite Hydrogels (MITCH) of alginate and a recombinant engineered protein (tropoelastin). Once mixed, the components formed a new gel-phase hydrogel with weak mechanical properties but which prevents cell sedimentation while maintaining cell viability during extrusion. The MITCH-Alginate ink was extruded within a calcium ion solution for ink crosslinking and prevent cell dehydration before moving the construct to cell culture medium. MITCH-Alginate cellularized printed scaffolds showed high cell viability and stability of the construct organization after 7 days of culture. In the present review, this approach was named 3D plotting and classified in the active positive class.

5.2.4. GHost writing: Guest-host writing

As an upgrade of the GHost-writing technique (paragraph 3.2.2), Shi and coworkers [51] exploited the dynamic coordination chemistry. In this approach, a self-healing matrix is produced through the reversible dynamic ion chelation of calcium cation by bisphosphonate-functionalized hyaluronic acid. The weak bonds between calcium cation and bisphosphonate can be disturbed by shear, allowing these materials to be used as Freeform 3D printing matrices. The ink had the same chemical composition but with acrylamide functions added for its stabilization through UV photocrosslinking. Calcium cations complex the bisphosphonate groups and this interaction was the basis of the active property of the technique. After UV photocrosslinking, tubes constructs were retrieved from the matrix and rinsed using acidified aqueous buffer.

5.2.5. Platform-assisted 3D inkjet bioprinting

Platform-assisted 3D inkjet bioprinting is one-of-a-kind techniques in Freeform 3D printing. Xu and coworkers [25] proposed this technique where cell-laden sodium alginate bioink was inkjet bioprinted and solidified when in contact with an aqueous calcium solution matrix (**Figure 7E**). Between each sodium alginate layer, the building stage was lowered by 70 µm for layer immersion and solidification in the calcium solution. In a vascular tissue engineering application, complex tubular structures were Freeform printed and after 72h of incubation, high cell viability was obtained. Another study was based on this principle but in the reverse way [24], i.e. a calcium solution was inkjet printed within a sodium alginate solution. Porous structures allowing cell migration and attachment in the pores were thus Freeform printed to design cardiac patches.

5.2.6. SSC: Sub Surface Catalyzation

Sub Surface Catalyzation (SSC) technique was applied to active positive Freeform 3D printing and further developed by the Picsima company (Fripp Design and Research, UK) [8]. In this application of SCC, the matrix consists in two-part polyaddition silicone elastomer curing at room temperature when catalyst is added. The printing ink is the polyaddition platinum catalyst. The matrix contains a crosslinker that reacts *in-situ* with the extruded catalyst ink, generating the crosslinking of the silicone only at the extrusion point. After 10-30 minutes of curing within the silicone matrix, constructs such as silicone ear plugs, seals are obtained and removed and then were cleaned. Similarly, Greenwood and coworkers [8] performed the Freeform of silicone elastomer structures with silicone matrix trapped. To do so, they formulated a silicone matrix curing only in contact of the printed silicone ink, keeping the integrity of the matrix reservoir [8]. Yet the cured matrix is trapped inside but the ink-matrix adhesion is enhanced, keeping mechanical properties close to the cast ones and decreases printing time. In the present review, this approach was named sub surface catalysation and classified in the active positive class, even if some part of the matrix is being removed after printing.

6. Discussion and insights

The proposed classification in 6 classes, describing all the current techniques, enables their rapid understanding but also the uncovering of clusters, scattered across multiple classes (**Figure 1**).

A typical example is the FRESH technique found in active positive [11,16,118], passive positive [29] and active negative Freeform 3D printing [29]. In a similar way, the Emb3D/ODP (Embedded 3D printing/ Omnidirectional printing) was classified both in passive negative [13,27] and in passive null Freeform 3D printing classes [14,33,42,48].

More precisely, the FRE (Freeform Reversible Embedding) [11,16] /PTG (Printing-Then-Gelation) technique [17,63] appears to dominate the positive Freeform 3D printing class, with a high focus on bioprinting using active positive class where we can cite FRESH [16,18], AAFB (Aspiration-Assisted Freeform Bioprinting) [26,67] and BATE (Bioprinting-Assisted Tissue Emergence) [79]. These active positive techniques polarize toward bioprinting with the capability of the FRE/PTG to handle aqueous phases [16], use gelation mechanisms using crosslinkers from the matrix [17,107], maintain the osmotic pressure of the construct [39,124,125], leading then to high cell viability and even tissue maturation directly within the support matrix [70]. Thus FRESH, the most spread technique in bioprinting, mostly finds applications using hydrophilic materials for inks and matrices.

Concerning negative Freeform 3D printing, less methods have been proposed, although an increasing family of techniques is now gathered around the term Embedded 3D printing (Emb3D) [28,38,42] which seems to be adopted by the community. The main focus of negative Freeform 3D printing is the development of microfluidics [13,28] and perfused channels for tissue engineering [31,66] and vascularization [66,97].

Similarly, null Freeform 3D printing finds applications in the manufacture of fine and delicate tubular structures [44,46] or composite functional multimaterials from nonpolar matrices for robotics applications [14,42].

From a support matrix point of view, the vast majority of the Freeform 3D printing techniques are based on microgels or jammed particles [15]. These microgels are microsized polymers swelled and dispersed in a solvent that turn into a jammed state with a solid behavior when sufficient particle-to-volume fraction is reached. Carbopol®, made of swollen poly(acrylic acid), is here the most widely used material, thanks to its availability and

ease of preparation [11,12,26,61]. In FRESH method, gelatin is the preferred material, mainly because of its biocompatibility [16,118,122]. However, the preparation of gelatin microgels is laborious [30] even if recently, a coacervation approach enabled to obtain more reproducible microparticles and rheological properties [102]. Complementary but seldom approaches are now based on bulk hydrogel synthesis for the development of new materials characterized by low yield stress or low thixotropy [75]. One example of these approaches are the exploitation of supramolecular assemblies using reversible guest-host interactions [31,41,126], nanoparticle suspensions (laponite, fumed silica) [63,89–91]. These approaches are nevertheless still difficult to scale-up [17,30] and solvent and material residues potentially hinder intrinsic properties of the final 3D part [17,90]. Recently, recyclable and reusable matrices have been developed to limit the waste of non-reusable matrices. Examples of such eco-friendly approaches are reusable matrices of spherical microgels of calcium-chelated alginate (Direct Freeform 3D printing Process (DF3DP)) [20,69] in addition with glycerol as a humectant following with a rehydration step to ensure the recovery of initial properties. Another example is a silicone oil-in-water emulsion glass matrix [93] which consists of jammed silicone oil droplets at high volume fraction (over 85%) in a surfactant aqueous solution (sodium dodecyl sulfate). Stable for at least 3 months, the matrix is also reusable (at least 6 times) and recyclable by separating the silicone oil and water phases to fabricate a new emulsion glass. Finally, thermoreversible matrices made of Pluronic® F-127 (F127) can be used to manufacture complex shapes [13,50,115]. F127 is a amphiphilic triblock copolymer composed of poly(ethylene oxide) (PEO) and poly(propylene oxide) (PPO) in a PEO-PPO-PEO configuration. This material undergoes a reversible sol-gel transition triggered by temperature and concentration changes. At low temperatures, in aqueous solutions, the copolymer is fully hydrated, leading to a viscous material. The temperature increase causes micelle formation and with the micelle entanglement (above the critical gel concentration) a solid-like state with a yield stress behavior [50].

Table 1. Overview of the current Freeform 3D printing techniques with their classification, terms, and materials. The printing resolution is presented and those highlighted with an asterisk means values not available but approximated from the tip diameter used in the study.

Freeform 3D printing class	Freeform 3D printing subclass	Term	Matrix material	Ink material	Printing resolution (μm)	Applications	Refs.
Negative	Passive	**Emb3D/ODP**	F127-DA	F127	18	3D biomimetic vascular architectures	[13]
			Silicone	F127	75	Soft autonomous robots development, microfluidic logic	[27]
		FRE/PTG	Gellan or gelatin microparticles suspension in gelatin	alginate	750*	Perfused microfluidic channels in composite hydrogel matrices	[35]
			GelMA microparticles suspension in GelMA	F127	410*	Disease and tumor microenvironment modeling	[37]
		SWIFT	Cell Spheroids	Gelatin	200	Perfused vascular architectures in embryoid bodies and cardiac organoid	[38]
		-	Cellulose nanofiber hydrogel	Mineral oil, paraffin wax and liquid paraffin	125	Soft paper microfluidics, chemical detection	[28]
	Active	**FRESH**	Gelatin or alginate microparticles suspension	Xanthan gum	600*	Perfused microfluidic, vascular-mimetic architectures, tissue engineering	[29]
		Ghost-writing	Hyaluronic acid-based	Hyaluronic acid-based	35-400	Self-healing materials, perfused vascular architectures, personalized medicine, angiogenesis study	[31,41]
		-	Xanthan gum	Alginate	200	Perfused vascular architectures	[30]
Null	Passive	**Embedded droplet printing**	Carbopol®	Gallium-indium alloy	50	Liquid metal printing, stereo structural electronics	[43]
			Silicone	Aqueous solution, bacterial growth media	300	Microbatch chemical reactions and biological assays	[45]
		Emb3D/ODP	Silicone	Silicones, F127, Carbon conductive silicone oil, conductive ionogel	159-410	Soft robotics, actuators, phonomimetic human vocal fold models, fluid flow deformation, flexible wearable electronics	[14,33,42,48]
		Solid object sculpting	Carbopol®-blend	Silicone oil-water emulsion	100	Organ phantoms, pre-operative surgery guidance	[47]
			F127-PEG	Silicone elastomer	410		[49]

	Active	**FREAL**	PEO- fluid based	Dextran, PAA, PAAM, PVA	10	All-liquid complex vascular architectures, vascular tissue engineering	[44]
		Ghost-writing	Modified hyaluronic acid-based	Modified hyaluronic acid	35	Self-healing materials, hydrogel multimaterial extrusion, chemical gradients	[41,51]
		Reconfigurable printed liquids	Silicone oil-based	Nanoparticles aqueous suspension	10	All-liquid electronics, cell and material encapsulation, chemical synthesis and separation	[46]
Positive	Passive	**3D plotting**	Gelatin solution	Agar gel	150	Hydrogel printing, tissue engineering	[78]
			Water	Silicone	200	Silicone printing, biomedical applications	[77]
		AAFB	Carbopol®, alginate microparticles suspension, AD-HA/CD-HA	Spheroids	150-200	Bioprinting of spheroids, tissue engineering (bone, cartilage, cardiac), drug screening	[26,67]
		BATE	Matrigel™, collagen	Cells only	50	Cellular self-organization, vascular, epithelial and connective tissue engineering	[79]
		CLASS	Agarose microparticles suspension	Alginate; GelMA	305	Matrix development, cell-laden hydrogel printing	[68]
		DF3DP	Alginate microparticles suspension	Silicone	1000-1000	Flexible wearable, recyclable matrix development for industrial scale use	[20,69]
			Alginate microparticles suspension	Cells only	417	Matrix development, bone and cartilage tissue engineering	[70]
		EDIW	Hydrophobic fumed silica suspension	Inorganic loaded polymers (SiOC and Ti_2AlC), hydrophobic materials (PDMS, SU-8, epoxy-based conductive ink)	50-400	Metal, ceramic and hydrophobic materials printing, hydrophobic matrix development	[89–91]
		EIW	Fluid alcohol-based (methanol, ethanol, isopropanol)	Silicone	65	Silicone flexible wearables, microfluidics, soft robotic actuators	[92]
		Emulsion glass	Silicone Oil in water	Silicone	1830	Recyclable, UV and thermal resistant matrix development	[93]
		FRE/PTG	Alginate microparticles suspension in xanthan gum	Gelatin (sacrificial) omentum gel, cells (positive)	300	Cell-laden and personalized printed hydrogels, tissues and organs, drug screening	[66]

			Aqueous nanoclay suspension	SU-8;Epoxy resin (passive) alginate or gelatin and cells (active), alginate-gelatin blend	75-180	fluid flow deformation, matrix development, hydrogel and hydrophobic printing, printability, vascular tissue engineering	[63–65]
			Carbopol®	Silicone, PVA, PEG	100 - 1219*	Fluid flow deformation, low-cost equipment development, extrusion optimization, patient-Specific Wearable silicone Pulse Oximeter	[11,12,32,52–56]
			Carbopol®	Interpenetrating network hydrogels (gelatin methacrylate-alginate), concentrated cells pellet, collagen, bioelastomer (itaconic acid), PVA, PEO, gelatin and human recombinant elastin based	20-400	Cardiac, intestine, vascular, tumor tissue engineering, cell behavior in hydrogel matrix, interpenetrating polymer networks bioink development, porous bioelastomers, fluid instabilities in high speed process	[57–62]
			Gellan fluid gel, Laponite®	Gelatin, alginate, PEGDA	683	matrix development, cell-laden hydrogel constructs, biomedical applications	[17]
			Polyacrylamide microgel-based suspension	Collagen+cells	50-80	Intestine tissue engineering, cell generated forces in cell-laden printed hydrogels	[61,127]
		FRESH	Gelatin microparticles suspension	Oxidized methacrylated alginate (OMA) and cells, hyaluronic acid and collagen and cells, collagen and hydroxyapatite	120-300	Cryopreservation, bone and cartilage tissue engineering, 3D cancer drug screening, organoids on chip	[80–87]
			F127	Silicone and iron oxide nanoparticles	300	Soft silicone magnetic helical coil actuators, soft robotics	[88]
			F127-PEG	Silicone	200	Matrix development, fluid instabilities, pre-operative surgery guidance	[50]
		IBPC	Aqueous nanoclaysuspension	Carbon fiber reinforced epoxy	220	Thermosetting polymers printing, structural, aerospace components, fiber reinforced composites	[71]
		Micro-organogel support matrix	Hydrophobic block-copolymers (SEP-SEBS)	Silicone	80	Matrix development, fluid instabilities, perfused devices, phonomimetic human vocal fold models	[34,95]

		SLAM	Agarose microparticles suspension	Collagen, gellan gum, alginate, and i-carrageenan and cells, Laponite® and gellan gum and cells, blood derivatives (platelet lysate), gellan and hydroxyapatite, GelMA	102-250	Matrix and bioactive bioink development, anisotropic and gradient biological constructs, tissue engineering (bone, cartilage, vascular), angiogenesis, osteochondral plugs	[73–76]
		SMAP	PTFE particles	Bacterial cellulose hydrogel	500	Bacterial cellulose 3D fabrication and printing, vascular tissue engineering	[97]
		Freeform in a Supporting Viscous Liquid	Carboxymethyl cellulose	pNIPAM+pAAM	400	4d thermo-responsive hydrogels printing, soft actuators, robotics, self-assembly and adaptive systems	[94]
	Active	**3D plotting**	Calcium solution	MICTH alginate	246	Bioink development, tissue engineering	[123]
		Catalytically initiated gel-in-gel 3D printing	F127	F127-dimethacrylate	410	4D printing, photothermally responsive objects, stimuli-responsive actuators	[117]
		CLASS	Agarose microparticles suspension	Alginate	305	Matrix development, cell-laden hydrogel printing	[68]
		COBICS	Gelatin microparticles suspension	Calcium phosphate	200	Porous ceramic printing, bone tissue engineering	[118]
		Embedded droplet printing	Carbopol®	Pharmaceutical compounds	300	spherical crystallization of pharmaceutical particles	[45]
		FPP	Carbopol®	Solubilized thermoplastics (ABS, HIPS, PS, PLA, PCL, etc.)	200	Thermoplastic printing	[19]
		FRE/PTG	Aqueous nanoclay suspension	SU-8, Epoxy resin (passive), alginate or gelatin and cells (active), silk, gelatin-alginate	100-1000	Fluid flow deformation, matrix development for UV, ionic and thermal curing biomaterials, Silk printing, neuromuscular and vascular tissue engineering, printability of hydrogel constructs	[21,63,99]
			Gellan fluid gel, laponite	Gelatin, alginate, PEGDA	683	Matrix development, cell-laden hydrogel constructs, biomedical applications	[17]
			Xanthan gum	Alginate and cells (in positive)	200	Matrix development, hydrogel anatomical models, cell-laden printing	[30]

		FRESH	F127-based	Alginate-based	50-305	Matrix development, hydrogel extrusion, cell-laded hydrogel constructs, vascular tissue engineering	[72,115,116]
			Gelatin microparticles suspension	Hydrogels and cell-laden hydrogels (alginate, collagen, hyaluronic acid-base, etc.)	20-1000	Tissue engineering (corneal, heart, muscle, bone, neural, etc.), therapeutic applications, equipment hardware, food printing, implant cellularization, pre-operative surgery guidance	[18,101–114]
		Freeze-FRESH	Gelatin microparticles suspension	Alginate and hyaluronic acid, collagen	500	Porous hydrogel development by freeze-casting, breast cancer modelling	[119,120]
		Ghost-writing	HA-BP and Calcium	Am-HA-BP and Calcium	NA	Self-healing materials, ink and matrix development, tissue-mimicking constructs, biomedical applications	[51]
		***In-situ* precipitation-coupled FRESH 3D printing**	Gelatin microparticles suspension	Hyaluronic acid-alginate based	510	Ink and matrix development, ceramic *in-situ* composite precipitation, bone tissue engineering	[121]
		Multifunctional granular composite matrix	Gelatin microparticles suspension in oxidized alginate	Modified gelatin	500	Ink and matrix development, cell-laden hydrogel printing, tissue engineering	[100]
		Platform-assisted 3D inkjet bioprinting	Alginate solution	Calcium solution	100	Inkjet bioprinting, vascular and cardiac tissue engineering	[24]
			Calcium solution	Alginate	106	Inkjet bioprinting, vascular tissue engineering	[25]
		SSC	Silicone	Silicone	260	Prostheses, Low solid-infill and low-stiffness silicone printing	[8,128]
		Submerged 3D bioprinting	Fluorocarbon liquid	Agarose	575	Cell-laden hydrogel bioink, tissue engineering, regenerative medicine	[98]
		TMF bioprinting	Gelatin microparticles suspension	Chitosan	150	Porous cell-laden hydrogel development, vocal fold tissue engineering, cancer modelling	[122]

7. Conclusion

In this review, the existing techniques involving Freeform 3D printing, *i.e.* printing liquid materials within a temporary or permanent support matrix, were presented and classified. Depending on the final product, Freeform 3D printing techniques were classified into negative, null and positive Freeform 3D printing. Then, depending on the chemical interaction between ink and matrix, the techniques were also classified into passive and active Freeform 3D printing. The proposed 6 classes' classification uses generic terms to describe all the current techniques and enables their rapid understanding but also the uncovering of clusters, scattered across multiple classes. For a better reading of the present classification, synthetic and didactic diagram was constructed. Some classes were found to be in their early stage (*e.g.* Null-Passive class) or even not studied yet (*e.g.* Negative-Active class), while some others were gathered into large clusters. These gaps and popularities were analyzed and discussed and it is foreseen that the proposed classification will have a positive impact into the scientific community to go further in materials innovation.

References

1. A. Shapira, N. Noor, M. Asulin, and T. Dvir, Appl. Phys. Rev. **5**, 041112 (2018).
2. S. Chen, W. S. Tan, M. A. Bin Juhari, Q. Shi, X. S. Cheng, W. L. Chan, and J. Song, Biomed. Eng. Lett. **10**, 453 (2020).
3. M. Vaezi, H. Seitz, and S. Yang, Int. J. Adv. Manuf. Technol. **67**, 1721 (2013).
4. R. L. Truby and J. A. Lewis, Nature **540**, 371 (2016).
5. C. A. Mandon, L. J. Blum, and C. A. Marquette, Anal. Chem. **88**, 10767 (2016).
6. J. Plott, X. Tian, and A. Shih, J. Manuf. Sci. Eng. **140**, (2018).
7. E.-J. Courtial, C. Perrinet, A. Colly, D. Mariot, J.-M. Frances, R. Fulchiron, and C. Marquette, Addit. Manuf. **28**, 50 (2019).
8. T. E. Greenwood, S. E. Hatch, M. B. Colton, and S. L. Thomson, Addit. Manuf. **37**, 101681 (2021).
9. A. GhavamiNejad, N. Ashammakhi, X. Y. Wu, and A. Khademhosseini, Small **16**, 2002931 (2020).
10. C. S. O'Bryan, T. Bhattacharjee, S. R. Niemi, S. Balachandar, N. Baldwin, S. T. Ellison, C. R. Taylor, W. G. Sawyer, and T. E. Angelini, MRS Bull. **42**, 571 (2017).
11. T. J. Hinton, A. Hudson, K. Pusch, A. Lee, and A. W. Feinberg, ACS Biomater. Sci. Eng. **2**, 1781 (2016).
12. T. Bhattacharjee, S. M. Zehnder, K. G. Rowe, S. Jain, R. M. Nixon, W. G. Sawyer, and T. E. Angelini, Sci. Adv. **1**, (2015).
13. Wu Willie, DeConinck Adam, and Lewis Jennifer A., Adv. Mater. **23**, H178 (2011).
14. M. J. T., Vogt Daniel M., Truby Ryan L., Mengüç Yiğit, Kolesky David B., Wood Robert J., and Lewis Jennifer A., Adv. Mater. **26**, 6307 (2014).
15. W. Cheng, J. Zhang, J. Liu, and Z. Yu, View **1**, 20200060 (2020).
16. D. J. Shiwarski, A. R. Hudson, J. W. Tashman, and A. W. Feinberg, APL Bioeng. **5**, 010904 (2021).
17. A. M. Compaan, K. Song, and Y. Huang, ACS Appl. Mater. Interfaces **11**, 5714 (2019).
18. T. J. Hinton, Q. Jallerat, R. N. Palchesko, J. H. Park, M. S. Grodzicki, H.-J. Shue, M. H. Ramadan, A. R. Hudson, and A. W. Feinberg, Sci. Adv. **1**, e1500758 (2015).
19. R. Karyappa and M. Hashimoto, ACS Appl. Polym. Mater. **3**, 908 (2021).
20. W. S. Tan, M. A. B. Juhari, Q. Shi, S. Chen, D. Campolo, and J. Song, Addit. Manuf. **36**, 101563 (2020).
21. M. J. Rodriguez, T. A. Dixon, E. Cohen, W. Huang, F. G. Omenetto, and D. L. Kaplan, Acta Biomater. **71**, 379 (2018).
22. K. N. Kalashnikov, V. E. Rubtsov, N. L. Savchenko, T. A. Kalashnikova, K. S. Osipovich, A. A. Eliseev, and A. V. Chumaevskii, Int. J. Adv. Manuf. Technol. **105**, 3147 (2019).
23. Y. Li, K. Tang, D. He, and X. Wang, Comput.-Aided Des. **133**, 102986 (2021).
24. T. Boland, X. Tao, B. J. Damon, B. Manley, P. Kesari, S. Jalota, and S. Bhaduri, Mater. Sci. Eng. C **27**, 372 (2007).
25. C. Xu, W. Chai, Y. Huang, and R. R. Markwald, Biotechnol. Bioeng. **109**, 3152 (2012).
26. B. Ayan, N. Celik, Z. Zhang, K. Zhou, M. H. Kim, D. Banerjee, Y. Wu, F. Costanzo, and I. T. Ozbolat, Commun. Phys. **3**, 1 (2020).
27. M. Wehner, R. L. Truby, D. J. Fitzgerald, B. Mosadegh, G. M. Whitesides, J. A. Lewis, and R. J. Wood, Nature **536**, 451 (2016).
28. S. Shin and J. Hyun, ACS Appl. Mater. Interfaces **9**, 26438 (2017).
29. G. Štumberger and B. Vihar, Mater. Basel Switz. **11**, (2018).
30. S. G. Patrício, L. R. Sousa, T. R. Correia, V. M. Gaspar, L. S. Pires, J. L. Luís, J. M. Oliveira, and J. F. Mano, Biofabrication **12**, 035017 (2020).
31. K. H. Song, C. B. Highley, A. Rouff, and J. A. Burdick, Adv. Funct. Mater. **28**, 1801331 (2018).
32. K. J. LeBlanc, S. R. Niemi, A. I. Bennett, K. L. Harris, K. D. Schulze, W. G. Sawyer, C. Taylor, and T. E. Angelini, ACS Biomater. Sci. Eng. **2**, 1796 (2016).
33. A. K. Grosskopf, R. L. Truby, H. Kim, A. Perazzo, J. A. Lewis, and H. A. Stone, ACS Appl. Mater. Interfaces (2018).
34. C. S. O'Bryan, T. Bhattacharjee, S. Hart, C. P. Kabb, K. D. Schulze, I. Chilakala, B. S. Sumerlin, W. G. Sawyer, and T. E. Angelini, Sci. Adv. **3**, e1602800 (2017).

35. A. M. Compaan, K. Song, W. Chai, and Y. Huang, ACS Appl. Mater. Interfaces **12**, 7855 (2020).
36. N. Nio, M. Motoki, and K. Takinami, Agric. Biol. Chem. **50**, 851 (1986).
37. T. G. Molley, G. K. Jalandhra, S. R. Nemec, A. S. Tiffany, A. Patkunarajah, K. Poole, B. A. C. Harley, T. Hung, and K. A. Kilian, Biomater. Sci. **9**, 4496 (2021).
38. M. A. Skylar-Scott, S. G. M. Uzel, L. L. Nam, J. H. Ahrens, R. L. Truby, S. Damaraju, and J. A. Lewis, Sci. Adv. **5**, eaaw2459 (2019).
39. A. McCormack, C. B. Highley, N. R. Leslie, and F. P. W. Melchels, Trends Biotechnol. (2020).
40. A. F. Dário, L. M. A. Hortêncio, M. R. Sierakowski, J. C. Q. Neto, and D. F. S. Petri, Carbohydr. Polym. **84**, 669 (2011).
41. C. B. Highley, C. B. Rodell, and J. A. Burdick, Adv. Mater. **27**, 5075 (2015).
42. R. L. Truby, M. Wehner, A. K. Grosskopf, D. M. Vogt, S. G. M. Uzel, R. J. Wood, and J. A. Lewis, Adv. Mater. **30**, 1706383 (2018).
43. Y. Yu, F. Liu, R. Zhang, and J. Liu, Adv. Mater. Technol. **2**, 1700173 (2017).
44. G. Luo, Y. Yu, Y. Yuan, X. Chen, Z. Liu, and T. Kong, Adv. Mater. **31**, 1904631 (2019).
45. A. Z. Nelson, B. Kundukad, W. K. Wong, S. A. Khan, and P. S. Doyle, Proc. Natl. Acad. Sci. **117**, 5671 (2020).
46. J. Forth, X. Liu, J. Hasnain, A. Toor, K. Miszta, S. Shi, P. L. Geissler, T. Emrick, B. A. Helms, and T. P. Russell, Adv. Mater. **30**, 1707603 (2018).
47. J. Zhao, M. Hussain, M. Wang, Z. Li, and N. He, Addit. Manuf. **32**, 101097 (2020).
48. T. E. Greenwood and S. L. Thomson, J. Biomech. 110388 (2021).
49. A. Tejo-Otero, A. Colly, E.-J. Courtial, F. Fenollosa-Artés, I. Buj-Corral, and C. A. Marquette, Rapid Prototyp. J. **ahead-of-print**, (2021).
50. A. Colly, C. Marquette, and E.-J. Courtial, Langmuir **37**, 4154 (2021).
51. L. Shi, H. Carstensen, K. Hölzl, M. Lunzer, H. Li, J. Hilborn, A. Ovsianikov, and D. A. Ossipov, Chem. Mater. **29**, 5816 (2017).
52. S. Abdollahi, A. Davis, J. H. Miller, and A. W. Feinberg, PloS One **13**, e0194890 (2018).
53. MenonAditya, PóczosBarnabás, F. W, and W. R, 3D Print. Addit. Manuf. (2019).
54. K. Hajash, B. Sparrman, C. Guberan, J. Laucks, and S. Tibbits, 3D Print. Addit. Manuf. **4**, 123 (2017).
55. A. McGhee, A. Bennett, P. Ifju, G. W. Sawyer, and T. E. Angelini, Exp. Mech. **58**, 137 (2018).
56. S. Abdollahi, E. J. Markvicka, C. Majidi, and A. W. Feinberg, Adv. Healthc. Mater. **9**, 1901735 (2020).
57. H. Savoji, L. Davenport Huyer, M. H. Mohammadi, B. F. Lun Lai, N. Rafatian, D. Bannerman, M. Shoaib, E. R. Bobicki, A. Ramachandran, and M. Radisic, ACS Biomater. Sci. Eng. **6**, 1333 (2020).
58. S. Krishnamoorthy, Z. Zhang, and C. Xu, J. Biomater. Appl. **33**, 1105 (2019).
59. S. Lee, E. S. Sani, A. R. Spencer, Y. Guan, A. S. Weiss, and N. Annabi, Adv. Mater. **32**, 2003915 (2020).
60. T. Bhattacharjee, C. J. Gil, S. L. Marshall, J. M. Urueña, C. S. O'Bryan, M. Carstens, B. Keselowsky, G. D. Palmer, S. Ghivizzani, C. P. Gibbs, W. G. Sawyer, and T. E. Angelini, ACS Biomater. Sci. Eng. **2**, 1787 (2016).
61. Y. Zhang, S. T. Ellison, S. Duraivel, C. D. Morley, C. R. Taylor, and T. E. Angelini, Bioprinting **21**, e00121 (2021).
62. Y. Jin, A. Compaan, T. Bhattacharjee, and Y. Huang, Biofabrication **8**, 025016 (2016).
63. Y. Jin, A. Compaan, W. Chai, and Y. Huang, ACS Appl. Mater. Interfaces **9**, 20057 (2017).
64. Y. Jin, W. Chai, and Y. Huang, Mater. Sci. Eng. C **80**, 313 (2017).
65. H. Ding and R. C. Chang, Appl. Sci. **8**, 403 (2018).
66. N. Noor, A. Shapira, R. Edri, I. Gal, L. Wertheim, and T. Dvir, Adv. Sci. **6**, 1900344 (2019).
67. A. C. Daly, M. D. Davidson, and J. A. Burdick, Nat. Commun. **12**, 753 (2021).
68. E. Mirdamadi, N. Muselimyan, P. Koti, H. Asfour, and N. Sarvazyan, 3D Print. Addit. Manuf. **6**, 158 (2019).
69. W. S. Tan, Q. Shi, S. Chen, M. A. Bin Juhari, and J. Song, Biomed. Eng. Lett. **10**, 517 (2020).
70. O. Jeon, Y. B. Lee, H. Jeong, S. J. Lee, D. Wells, and E. Alsberg, Mater. Horiz. **6**, 1625 (2019).
71. M. Mahmoudi, S. R. Burlison, S. Moreno, and M. Minary-Jolandan, ACS Appl. Mater. Interfaces (2021).

72. F. Afghah, M. Altunbek, C. Dikyol, and B. Koc, Sci. Rep. **10**, 5257 (2020).
73. S. R. Moxon, M. E. Cooke, S. C. Cox, M. Snow, L. Jeys, S. W. Jones, A. M. Smith, and L. M. Grover, Adv. Mater. **29**, 1605594 (2017).
74. G. Cidonio, M. Cooke, M. Glinka, J. I. Dawson, L. Grover, and R. O. C. Oreffo, Mater. Today Bio **4**, 100028 (2019).
75. J. J. Senior, M. E. Cooke, L. M. Grover, and A. M. Smith, Adv. Funct. Mater. **29**, 1904845 (2019).
76. B. B. Mendes, M. Gómez-Florit, A. G. Hamilton, M. S. Detamore, R. M. A. Domingues, R. L. Reis, and M. E. Gomes, Biofabrication **12**, 015012 (2019).
77. R. Landers and R. Mülhaupt, Macromol. Mater. Eng. **282**, 17 (2000).
78. R. Landers, U. Hübner, R. Schmelzeisen, and R. Mülhaupt, Biomaterials **23**, 4437 (2002).
79. J. A. Brassard, M. Nikolaev, T. Hübscher, M. Hofer, and M. P. Lutolf, Nat. Mater. **20**, 22 (2021).
80. G. Montalbano, G. Molino, S. Fiorilli, and C. Vitale-Brovarone, J. Eur. Ceram. Soc. **40**, 3689 (2020).
81. G. Montalbano, G. Borciani, G. Cerqueni, C. Licini, F. Banche-Niclot, D. Janner, S. Sola, S. Fiorilli, M. Mattioli-Belmonte, G. Ciapetti, and C. Vitale-Brovarone, Nanomaterials **10**, 1681 (2020).
82. O. Jeon, Y. Bin Lee, T. J. Hinton, A. W. Feinberg, and E. Alsberg, Mater. Today Chem. **12**, 61 (2019).
83. E. Maloney, C. Clark, H. Sivakumar, K. Yoo, J. Aleman, S. A. P. Rajan, S. Forsythe, A. Mazzocchi, A. W. Laxton, S. B. Tatter, R. E. Strowd, K. I. Votanopoulos, and A. Skardal, Micromachines **11**, 208 (2020).
84. Kupfer Molly E., Lin Wei-Han, Ravikumar Vasanth, Qiu Kaiyan, Wang Lu, Gao Ling, Bhuiyan Didarul B., Lenz Megan, Ai Jeffrey, Mahutga Ryan R., Townsend DeWayne, Zhang Jianyi, McAlpine Michael C., Tolkacheva Elena G., and Ogle Brenda M., Circ. Res. **127**, 207 (2020).
85. E. L. Maxson, M. D. Young, C. Noble, J. L. Go, B. Heidari, R. Khorramirouz, D. W. Morse, and A. Lerman, Bioprinting **16**, e00059 (2019).
86. C. Noble, E. L. Maxson, A. Lerman, and M. D. Young, J. Mech. Behav. Biomed. Mater. **102**, 103519 (2020).
87. Y.-J. Choi, Y.-J. Jun, D. Y. Kim, H.-G. Yi, S.-H. Chae, J. Kang, J. Lee, G. Gao, J.-S. Kong, J. Jang, W. K. Chung, J.-W. Rhie, and D.-W. Cho, Biomaterials **206**, 160 (2019).
88. R. Bayaniahangar, S. Bayani Ahangar, Z. Zhang, B. P. Lee, and J. M. Pearce, Sens. Actuators B Chem. **326**, 128781 (2021).
89. K. Huang, H. Elsayed, G. Franchin, and P. Colombo, Appl. Mater. Today **23**, 101005 (2021).
90. M. Mahmoudi, C. Wang, S. Moreno, S. R. Burlison, D. Alatalo, F. Hassanipour, S. E. Smith, M. Naraghi, and M. Minary - Jolandan, ACS Appl. Mater. Interfaces **12**, 31984 (2020).
91. Y. Jin, K. Song, N. Gellermann, and Y. Huang, ACS Appl. Mater. Interfaces **11**, 29207 (2019).
92. R. Karyappa, T. Ching, and M. Hashimoto, ACS Appl. Mater. Interfaces **12**, 23565 (2020).
93. S.-W. Hu, P.-J. Sung, T. P. Nguyen, Y.-J. Sheng, and H.-K. Tsao, ACS Appl. Mater. Interfaces **12**, 24450 (2020).
94. T. Uchida and H. Onoe, Micromachines **10**, 433 (2019).
95. R. G. T. Romero, M. B. Colton, and S. L. Thomson, J. Voice (2020).
96. C. Marquette, E.-J. COURTIAL, A. DELBARRE, and A. COLLY, FR3089145A1 (5 June 2020).
97. S. Shin, H. Kwak, D. Shin, and J. Hyun, Nat. Commun. **10**, 4650 (2019).
98. D. F. D. Campos, A. Blaeser, M. Weber, J. Jäkel, S. Neuss, W. Jahnen-Dechent, and H. Fischer, Biofabrication **5**, 015003 (2012).
99. T. A. Dixon, E. Cohen, D. M. Cairns, M. Rodriguez, J. Mathews, R. R. Jose, and D. L. Kaplan, Tissue Eng. Part C Methods **24**, 346 (2018).
100. D. Heo, M. Alioglu, Y. Wu, V. Ozbolat, B. Ayan, M. Dey, Y. Kang, and I. Ozbolat, ACS Appl. Mater. Interfaces (2020).
101. E. Mirdamadi, J. W. Tashman, D. J. Shiwarski, R. N. Palchesko, and A. W. Feinberg, ACS Biomater. Sci. Eng. (2020).
102. A. Lee, A. R. Hudson, D. J. Shiwarski, J. W. Tashman, T. J. Hinton, S. Yerneni, J. M. Bliley, P. G. Campbell, and A. W. Feinberg, Science **365**, 482 (2019).
103. A. Isaacson, S. Swioklo, and C. J. Connon, Exp. Eye Res. **173**, 188 (2018).
104. J. Lewicki, J. Bergman, C. Kerins, and O. Hermanson, Bioprinting **16**, e00053 (2019).

105. M. Bordoni, E. Karabulut, V. Kuzmenko, V. Fantini, O. Pansarasa, C. Cereda, and P. Gatenholm, Cells **9**, 682 (2020).
106. S. M. Park, H. W. Kim, and H. J. Park, J. Food Eng. **271**, 109781 (2020).
107. S. M. Hull, C. D. Lindsay, L. G. Brunel, D. J. Shiwarski, J. W. Tashman, J. G. Roth, D. Myung, A. W. Feinberg, and S. C. Heilshorn, Adv. Funct. Mater. **31**, 2007983 (2021).
108. C. Aronsson, M. Jury, S. Naeimipour, F. R. Boroojeni, J. Christoffersson, P. Lifwergren, C.-F. Mandenius, R. Seleg\aard, and D. Aili, Biofabrication **12**, 035031 (2020).
109. A. Pellegrino, Undergrad. Res. Scholarsh. Symp. (2021).
110. F. Kreimendahl, C. Kniebs, A. M. Tavares Sobreiro, T. Schmitz-Rode, S. Jockenhoevel, and A. L. Thiebes, J. Appl. Biomater. Funct. Mater. **19**, 22808000211028810 (2021).
111. J. M. Bone, C. M. Childs, A. Menon, B. Póczos, A. W. Feinberg, P. R. LeDuc, and N. R. Washburn, ACS Biomater. Sci. Eng. **6**, 7021 (2020).
112. N. Bessler, D. Ogiermann, M.-B. Buchholz, A. Santel, J. Heidenreich, R. Ahmmed, H. Zaehres, and B. Brand-Saberi, HardwareX **6**, e00069 (2019).
113. E. M. Shen and K. E. McCloskey, Bioprinting **21**, e00113 (2021).
114. J. W. Tashman, D. J. Shiwarski, and A. W. Feinberg, HardwareX **9**, e00170 (2021).
115. M. Rocca, A. Fragasso, W. Liu, M. A. Heinrich, and Y. S. Zhang, SLAS Technol. **23**, 154 (2018).
116. W. Liu, Y. S. Zhang, M. A. Heinrich, F. D. Ferrari, H. L. Jang, S. M. Bakht, M. M. Alvarez, J. Yang, Y.-C. Li, G. T. Santiago, A. K. Miri, K. Zhu, P. Khoshakhlagh, G. Prakash, H. Cheng, X. Guan, Z. Zhong, J. Ju, G. H. Zhu, X. Jin, S. R. Shin, M. R. Dokmeci, and A. Khademhosseini, Adv. Mater. **29**, 1604630 (2017).
117. A. Basu, A. Saha, C. Goodman, R. T. Shafranek, and A. Nelson, ACS Appl. Mater. Interfaces **9**, 40898 (2017).
118. S. Romanazzo, T. G. Molley, S. Nemec, K. Lin, R. Sheikh, J. J. Gooding, B. Wan, Q. Li, K. A. Kilian, and I. Roohani, Adv. Funct. Mater. **n/a**, 2008216 (2021).
119. Z. Wang and S. J. Florczyk, Materials **13**, 354 (2020).
120. T. Sousa, N. Kajave, P. Dong, L. Gu, S. Florczyk, and V. Kishore, 3D Print. Addit. Manuf. (2021).
121. S. Chen, T.-S. Jang, H. M. Pan, H.-D. Jung, M. W. Sia, S. Xie, Y. Hang, S. K. M. Chong, D. Wang, and J. Song, Int. J. Bioprinting **6**, 22 (2020).
122. G. Bao, T. Jiang, H. Ravanbakhsh, A. Reyes, Z. Ma, M. Strong, H. Wang, J. M. Kinsella, J. Li, and L. Mongeau, Mater. Horiz. **7**, 2336 (2020).
123. K. Dubbin, Y. Hori, K. K. Lewis, and S. C. Heilshorn, Adv. Healthc. Mater. **5**, 2488 (2016).
124. C. S. O'Bryan, C. P. Kabb, B. S. Sumerlin, and T. E. Angelini, ACS Appl. Bio Mater. **2**, 1509 (2019).
125. C. S. O'Bryan, T. Bhattacharjee, S. L. Marshall, W. Gregory Sawyer, and T. E. Angelini, Bioprinting **11**, e00037 (2018).
126. C. B. Highley, K. H. Song, A. C. Daly, and J. A. Burdick, Adv. Sci. **6**, 1801076 (2019).
127. C. D. Morley, S. T. Ellison, T. Bhattacharjee, C. S. O'Bryan, Y. Zhang, K. F. Smith, C. P. Kabb, M. Sebastian, G. L. Moore, K. D. Schulze, S. Niemi, W. G. Sawyer, D. D. Tran, D. A. Mitchell, B. S. Sumerlin, C. T. Flores, and T. E. Angelini, Nat. Commun. **10**, 3029 (2019).
128. Picsima3d (n.d.).